 doi:10.20944/preprints202009.0532.v2

First immunohistochemical evidence of human tendon repair following stem cell injection: A case report and review of literature

Eckhard U. Alt[1,2,3] | *Ralf Rothoerl*[1] | *Matthias Hoppert*[1] | *Hans-Georg Frank*[4] | *Tobias Wuerfel*[4] | *Christopher Alt*[5] | *Christoph Schmitz*[4]

[1] *Isar Klinikum, Munich, Germany*
[2] *Sanford Health, Sioux Falls, SD, USA*
[3] *InGeneron, Inc., Houston, TX, USA*
[4] *Chair of Neuroanatomy, Institute of Anatomy, Faculty of Medicine, LMU Munich, Munich, Germany*
[5] *InGeneron GmbH, Munich, Germany*

Key words: adipose derived regenerative cells; ADRCs; efficacy; point of care treatment; stem cells; stromal vascular fraction; tendon healing without scar formation; tendon regeneration

Current clinical treatment options for symptomatic, partial-thickness rotator cuff tear (sPTRCT) offer only limited potential for true tissue healing and improvement of clinical results. In animal models, injections of adult stem cells isolated from adipose tissue into tendon injuries evidenced histological regeneration of tendon tissue. However, it is unclear whether such beneficial effects could also be observed in a human tendon treated with fresh, uncultured, autologous, adipose derived regenerative cells (UA-ADRCs). A specific challenge in this regard is that UA-ADRCs cannot be labeled and, thus, not unequivocally identified in the host tissue. Therefore, histological regeneration of injured human tendons after injection of UA-ADRCs must be assessed using comprehensive, immunohistochemical and microscopic analysis of biopsies taken from the treated tendon a few weeks after injection of UA-ADRCs.

Correspondence
Dr. Eckhard U. Alt MD, PhD
IsarKlinikum Munich
Sonnenstr. 24
80331 Munich
Germany
Phone: +1-832-853-3898
e.alt@biomed-science.com

 doi:10.20944/preprints202009.0532.v2

ABSTRACT

Current clinical treatment options for symptomatic, partial-thickness rotator cuff tear (sPTRCT) offer only limited potential for true tissue healing and improvement of clinical results. In animal models, injections of adult stem cells isolated from adipose tissue into tendon injuries evidenced histological regeneration of tendon tissue. However, it is unclear whether such beneficial effects could also be observed in a human tendon treated with fresh, uncultured, autologous, adipose derived regenerative cells (UA-ADRCs). A specific challenge in this regard is that UA-ADRCs cannot be labeled and, thus, not unequivocally identified in the host tissue. Therefore, histological regeneration of injured human tendons after injection of UA-ADRCs must be assessed using comprehensive, immunohistochemical and microscopic analysis of biopsies taken from the treated tendon a few weeks after injection of UA-ADRCs.

INTRODUCTION

Symptomatic, partial-thickness rotator cuff tear (sPTRCT) is one of the most prevalent shoulder disorders in adults, often leading to persistent pain, loss of function and occupational disability[1]. Current non-surgical and surgical treatment options to address sPTRCT do not necessarily have the potential to replace damaged tendon tissue, and often do not improve clinical results[2]. Treatment with corticosteroid injection can provide short-term pain relief but may not modify the long-term course of the disease[2,3]. Two recent studies [a systematic review[4] and a randomized controlled trial (RCT)[5]] found that injections of platelet rich plasma might be of limited benefit in non-operative treatment of rotator cuff disease. Other authors demonstrated that results from surgical interventions may not exceed those obtained with conservative management[6].

Fresh, uncultured, autologous, adipose derived regenerative cells (UA-ADRCs) are prepared at the point of care (in some publications these cells are also called stromal vascular fraction; SVF)[7]. Unlike some other cell preparations currently under investigation for use in regenerative medicine (including bone marrow derived cells, allogenic stem cells, amniotic cells or induced pluripotent stem cells) UA-ADRCs are derived from the same patient, not expanded in culture and are less exposed to factors that could affect their safety and efficacy[7,8]. Furthermore, UA-ADRCs do not share the risk of potentially developing tumors and immunological defensive reactions[7]. While less than 0.1% of the total population of bone marrow nucleated cells represent true stem cells, UA-ADRCs contain up to 10% multipotent cells out of the total population of injected cells[7]. Additionally, harvesting adipose tissue is considered less invasive than harvesting bone marrow[9].

A recent *in vitro* study demonstrated that fresh UA-ADRCs may be superior to cultured adipose derived stem cells (ADSCs) as trophic mediators for tendon healing[10]. In addition, we recently published the first-in-human pilot RCT on treating sPTRCT with UA-ADRCs[11]. In the latter study patients treated with injection of UA-ADRCs showed significant clinical improvement compared to patients treated with corticosteroid injection ($P < 0.05$) at six and twelve months post treatment[11].

The aim of the present, comprehensive immunohistochemical and microscopic analysis of a biopsy of the supraspinatus tendon of a patient suffering from sPTRCT (taken ten weeks after injection of the cells) is to provide novel insights into potential mechanisms of tendon regeneration following stem cell injection in humans. To our knowledge, this is the first investigation of a biopsy taken from a human tendon after application of unmodified, autologous stem cells.

This study is a single self-experiment with the patient's consent. The patient is the first author of this study, Alt E, MD, PhD. Single self-experiments with the patient's unrestricted and free will formation are exempt from approval of an Institutional Review Board in Germany[12]. It was Alt E himself who initiated his own treatment, taking the biopsy and all investigations. Alt E gave informed consent to participate in this study.

CASE PRESENTATION

Chief complaints

In October 2016 the then 66-year old patient experienced intense pain in his right shoulder with pain radiating to his back, upper arm and elbow.

History of present illness

The patient reported a bicycle accident a few days earlier, hitting the street with his right shoulder first.

History of past illness

No specific past illness or injury was reported that was directly related to the present illness.

Personal and family history

No specific personal and family history was reported that was directly related to the present illness.

Physical examination

The clinical examination upon admission revealed a painfully restricted mobility of the right shoulder and evidence pointing to injury of the rotator cuff. The American Shoulder and Elbow Surgeons Standardized Shoulder Assessment Form (ASES) total score of the right shoulder was 12 upon admission (the ASES total score of the left shoulder was 100, which is the highest score possible, indicating no shoulder pain and no impairment of shoulder mobility[13,14]). Clinical tests specifically designed to diagnose rotator cuff pathology (empty can, Neer, painful arc, external rotation lag sign and infraspinatus muscle strength test[15]) were positive on the injured right side and negative on the left side.

Laboratory examinations

No specific laboratory examinations were performed upon admission other than routine lab works.

Imaging examinations

Magnetic resonance imaging of the right shoulder [performed using a 1.5 Tesla magnetic resonance imaging (MRI) scanner; Magnetom Avanto; Siemens, Erlangen, Germany] evidenced a combined partial-thickness tear of the supraspinatus tendon (PASTA), an intramuscular cyst of the supraspinatus muscle and a partial-thickness tear of the infraspinatus tendon (Figure 1A-D).

MULTIDISCIPLINARY EXPERT CONSULTATION

Note that this multidisciplinary expert consultation took place in October 2016 and reflects the state of the literature at this time.

Preprints (www.preprints.org) | NOT PEER-REVIEWED | Posted: 28 June 2021 doi:10.20944/preprints202009.0532.v2

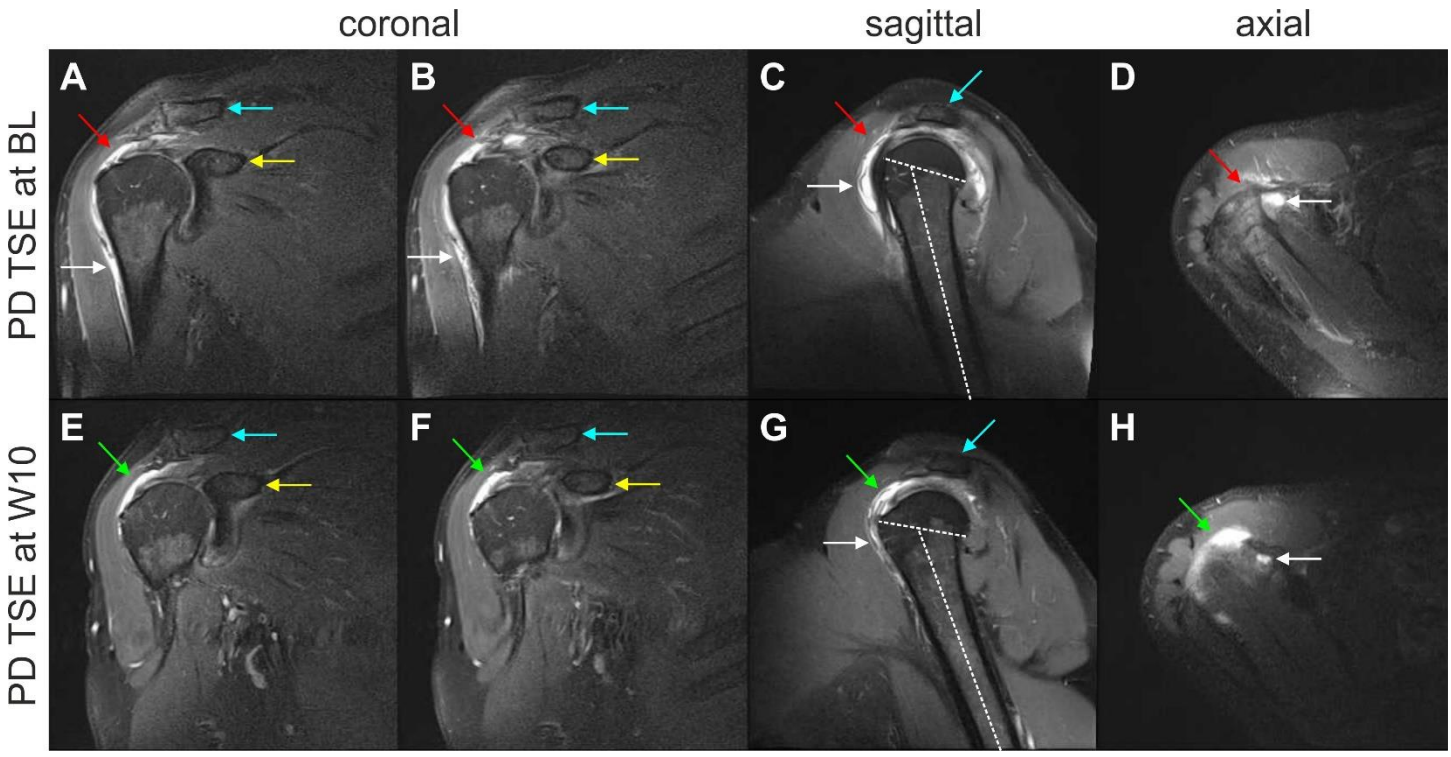

Figure 1 Proton density weighted, fat saturated, Turbo Spin Echo, 1.5 T magnetic resonance imaging scans of the right shoulder of the investigated patient (matrix 320 × 320; slice thickness 3 mm; inter-slice gap 0.3 mm; echo time 37 ms; repetition time 2450 ms at baseline and 3480 ms at ten weeks post injection). A and B: Coronal scans at baseline (BL) (white arrows, trauma-related bruising; red arrows, position of the supraspinatus tendon at which a hyperintense structure was found at ten weeks post injection (W10) but not at BL; blue arrows, clavicle; yellow arrows, coracoid process of the scapula); C: Sagittal scan at BL (white arrow, trauma-related bruising; red arrow, position of the supraspinatus tendon at which a hyperintense structure was found at W10 but not at BL; blue arrow, acromion; dotted lines, long axis of the humeral shaft and delineation of the humeral head, with same angle between the lines as in Panel G). D: Axial scan at BL (white arrow, trauma-related bruising; red arrow, position of the supraspinatus tendon at which a hyperintense structure was found at W10 but not at BL). E and F: Coronal scans at W10 (green arrows, hyperintense structure at the position of the supraspinatus tendon that was found at W10 but not at BL; blue arrows, clavicle; yellow arrows, coracoid process of the scapula); G: Sagittal scan at W10 (white arrow, trauma-related bruising; green arrow, hyperintense structure at the position of the supraspinatus tendon that was found at W10 but not at BL; blue arrow, acromion; dotted lines, long axis of the humerus and delineation of the humeral head, with same angle between the lines as in Panel C); H: Axial scan at W10 (white arrow, trauma-related bruising; green arrow, hyperintense structure at the position of the supraspinatus tendon that was found at W10 but not at BL). BL, baseline; PD TSE, proton density weighted turbo spin echo; W10; ten weeks post injection.

Matthias Hoppert, MD, Head of the Department for Orthopedics and Trauma Surgery, Isar Klinikum (Munich, Germany) and Ralf Rothoerl, MD, Head of the Department of Spine Surgery, Isar Klinikum (Munich, Germany)

The clinical and radiological findings outlined above suggest that usual conservative measures (including physical therapy and physiotherapy) will most probably not be successful in this case. Subacromial injection of corticosteroid may provide short-term pain relief, but may not result in tendon regeneration[2]. Even worse, subacromial injection of corticosteroid may potentially lead to tendon rupture[16]. Furthermore, surgical treatment has some risk of developing complications, may result in a lengthy recovery, and the clinical outcome may not be superior to clinical outcome after conservative management[17]. In summary, the case presented here is a borderline case that may be suitable for a regenerative therapy approach.

Eckhard U Alt, MD, PhD, Professor, Chairman of the Board of Isar Klinikum (Munich, Germany) and Executive Chair of InGeneron, Inc. (Houston, TX, United States)

To my knowledge reports about treatment of partial-thickness rotator cuff tears with injection of stem cells have not yet been published. On the other hand, basic research performed in our own and many other laboratories during the last years has demonstrated that ADSCs could regenerate injured human tendons. Specifically, these cells can engraft and survive in the new host tissue, integrate into and communicate within the new host tissue by forming direct cell-cell contacts, induce immune-modulatory and anti-inflammatory properties, protect cells at risk in the new host tissue from undergoing apoptosis, positively influence the new host tissue by release of cytokines (including insulin-like growth factor 1 and vascular endothelial growth factor), participate in building new vascular structures in the host tissue and differentiate

under guidance of the new microenvironment into cells of all three germ layers [7]. As it concerned my own shoulder, I agreed to treat the partial-thickness supraspinatus tendon tear with UA-ADRCs.

Christopher Alt, MD, Director of Science and Research of InGeneron GmbH (Munich, Germany) and SciCoTec (Grünwald, Germany)

So far, three studies addressing treatment of sPTRCT with stem cells have been published[18-20]. However, in these studies bone-marrow derived mesenchymal stem cells (BM-MSCs) rather than UA-ADRCs were applied. Furthermore, in these studies BM-MSCs were not used as the only therapy but to augment arthroscopic rotator cuff repair. Consequently, treating the sPTRCT of the patient discussed here with UA-ADRCs would represent a first-in-human case.

Hans-Georg Frank, MD and Christoph Schmitz, MD, Professors of Anatomy at LMU Munich (Munich, Germany), and Tobias Wuerfel, MS, Specialist in Quantitative Histology, LMU Munich (Munich, Germany)

By definition, UA-ADRCs cannot be labeled because this would render them modified. As a result, UA-ADRCs cannot be unequivocally identified in the host tissue. Therefore, histological regeneration of injured human tendons after injection of UA-ADRCs must be assessed using comprehensive, immunohistochemical and microscopic analysis of biopsies taken from the treated tendon a few weeks after application of UA-ADRCs. We are convinced that results of such quantitative and qualitative studies will be of great significance to the field, even if the results will only allow to draw indirect conclusions with regard to potential mechanisms of action of UA-ADRCs in the treatment of human tendon pathologies. To our knowledge, analyses of biopsies of injured human tendons after application of mesenchymal stem cells have not yet been published.

FINAL DIAGNOSIS

Symptomatic, combined PASTA, intramuscular cyst of the supraspinatus muscle and partial-thickness tear of the infraspinatus tendon, caused by an accident.

TREATMENT

On day 18 post injury (day 16 post MRI) the patient was treated by transcutaneous injection of UA-ADRCs adjacent to the supraspinatus tendon lesion under control of biplanar X-ray imaging. As part of this process, approximately 100 g of abdominal adipose tissue was harvested by liposuction, from which approximately 75×10^6 UA-ADRCs were isolated within less than two hours using the Transpose RT /Matrase system (InGeneron, Houston, TX, United States). Detailed characterizations of cells isolated from human adipose tissue using the Transpose RT /Matrase system (InGeneron) are available in the literature[7]. The UA-ADRCs were injected adjacent to the injured supraspinatus tendon immediately after isolation. The infraspinatus tendon was not treated at this time.

A control MRI performed ten weeks post treatment showed substantial reduction of trauma-related bruising and the formation of a hyperintense structure at the supraspinatus site of injection of the cells (Figure 1E-H). At this time the ASES total score had increased from 12 at baseline to 79, indicating clinical efficacy of the initial treatment. On the other hand, the control MRI indicated aggravation of the infraspinatus tendon tear of the right shoulder that required surgical revision. During this operation a biopsy (separated into two parts) from the supraspinatus tendon (at the position of the hyperintense structure that was seen on the MRI scans) was taken, which was then prepared for histological and immunohistochemical analysis. Since an open revision was already carried out anyway and in order to avoid any risk, the surgeons decided to surgically revise the supraspinatus tendon as well. Of note, this decision was made on the basis of the very limited knowledge about efficacy and safety of treating sPTRCT with injection of UA-ADRCs that was available in October 2016. Since then our knowledge about efficacy and safety of treating sPTRCT with injection of UA-ADRCs has greatly improved[11]. In case this knowledge would have been available in October 2016 the surgeons may have left the supraspinatus tendon untouched during the operation.

OUTCOME AND FOLLOW-UP

After fixation in 4% formaldehyde the two parts of the biopsy were separately embedded in paraffin and cut into 4 µm-thick tissue sections that were mounted on glass slides and stained with Azan trichrome stain or processed with immunohistochemistry. The latter was performed on de-paraffinized and rehydrated sections that were washed with phosphate buffered saline (PBS) containing Tween 20 (Sigma Aldrich, St. Louis, MO, United States). After antigen retrieval and / or enzymatic and / or chemical pretreatment the slides were blocked with different solutions for 15 min to 60 min at room temperature (details are provided in Table 1). Then, sections were incubated with primary antibodies for the detection of aggrecan, CD34, CD68, Ki-67, laminin, matrix metalloproteinase (MMP)-2, MMP-9, procollagen 1, tenomodulin, type I collagen, type II collagen, type III collagen and type IV collagen as summarized in Table 1.

Antibody binding was detected with the Vectastain Elite ABC Kit Peroxidase (HRP) (Vector Laboratories, Burlingame, CA, United States) with a secondary antibody incubation of 30 min for all slides (Table 1). Visualization of peroxidase activity was performed using diaminobenzidine (Vector Impact DAB chromogen solution; Vector Laboratories), resulting in a brown staining product. Mayer's hematoxylin was used for counterstaining the sections. In order to perform specificity controls primary antibodies were omitted and replaced with PBS. Microscopic evaluations were performed by Alt E, Frank HG, Alt C and Schmitz C.

Table 1 Characteristics of the antibodies used in the present study.

[1] The antibodies 12/21/1-C-6 (developed by Dr. Caterson B), 2E8 (developed by Dr. Engvall ES), CIIC1 (developed by Drs Holmdahl R and Rubin K) and SP1.D8 and M3F7 (developed by Dr. Furthmayr H) were obtained from the Developmental Studies Hybridoma Bank, created by the Eunice Kennedy Shriver National Institute of Child Health and Human Development of the National Institutes of Health of the United States, and maintained at The University of Iowa, Department of Biology, Iowa City, IA, United States; [2] Provider: Vector Laboratories (Burlingame, CA, United States). BSA, bovine serum albumin; DSHB, developmental studies hybridoma bank; GaM, goat anti-mouse; GaR, goat anti-rabbit; HaM, horse anti-mouse; HaR, horse anti-rabbit; IgG, immunoglobulin G; N/A, not applicable; NHS, normal horse serum; NGS, normal goat serum; PBS, phosphate-buffered saline.

Aggrecan	Immunoglobuline isotype / clone status	IgG1 / mouse, monoclonal
	Catalog no. / provider	12/21/1-C-6 / DSHB[1]
	Demasking of antigen	Protease XIV and Chondroitinase AC
	Blocking	Bloxall SP-6000[2], NHS S-2000[2], 1:20
	Dilution and incubation parameters	1:5, room temperature, 4 hours
	Secondary antibody used	HaM IgG BA-2000[2], 1:200
CD34	Immunoglobuline isotype / clone status	IgG1 / mouse, monoclonal
	Catalog no. / provider	QBEnd-10 / Thermo Scientific (Waltham, MA, United States)
	Demasking of antigen	N/A
	Blocking	3% H_2O_2 in methanol, NGS S-1000[2] 5 %
	Dilution and incubation parameters	1:900, 4 °C, overnight
	Secondary antibody used	GaM IgG BA-9200[2], 1:200, in 2% BSA/PBS
CD68	Immunoglobuline isotype / clone status	KP1- IgG1 kappa / mouse, monoclonal
	Catalog no. / provider	M0814 / Dako (Glostrup, Denmark)
	Demasking of antigen	Boiling in citrate buffer (pH 6)
	Blocking	Bloxall SP-6000[2], NHS S-2000[2], 1:20
	Dilution and incubation parameters	1:100, 4 °C, overnight
	Secondary antibody used	HaM IgG BA-2000[2], 1:200
Ki-67	Immunoglobuline isotype / clone status	MIB-1 IgG1 kappa / mouse, monoclonal
	Catalog no. / provider	M7240 / Dako (Glostrup, Denmark)
	Demasking of antigen	Boiling in citrate buffer (pH 6)
	Blocking	Bloxall SP-6000[2], NHS S-2000[2], 1:20
	Dilution and incubation parameters	1:75, 4 °C, overnight
	Secondary antibody used	HaM IgG BA-2000[2], 1:200
Laminin	Immunoglobuline isotype / clone status	IgG2a / mouse, monoclonal
	Catalog no. / provider	2E8 / DSHB[1]
	Demasking of antigen	N/A
	Blocking	3% H_2O_2 in methanol, NHS S-2000[2], 1:20
	Dilution and incubation parameters	1:5, room temperature, 30 minutes
	Secondary antibody used	HaM IgG BA-2000[2], 1:200
MMP-2	Immunoglobuline isotype / clone status	IgG / rabbit, polyclonal
	Catalog no. / provider	97779 / Abcam (Cambridge, MA)
	Demasking of antigen	N/A
	Blocking	Bloxall SP-6000[2], NGS S-1000[2], 1:20
	Dilution and incubation parameters	1:100, 4 °C, overnight
	Secondary antibody used	GaR IgG BA-1000[2], 1:200
MMP-9	Immunoglobuline isotype / clone status	IgG / rabbit, polyclonal
	Catalog no. / provider	38898 / Abcam
	Provider	Abcam
	Demasking of antigen	N/A
	Blocking	Bloxall SP-6000[2], NGS S-1000[2], 1:20
	Dilution and incubation parameters	1:100, 4 °C, overnight
	Secondary antibody used	GaR IgG BA-1000[2], 1:200
Procollagen 1	Immunoglobuline isotype / clone status	IgG1 / mouse, monoclonal
	Catalog no. / provider	SP1.D8 / DSHB[1]
	Demasking of antigen	Boiling in citrate buffer (pH 6)
	Blocking	Bloxall SP-6000[2], NHS S-2012[2], 2.5%
	Dilution and incubation parameters	1:10, 4 °C, overnight
	Secondary antibody used	HaM IgG BA-2000[2], 1:200
Tenomodulin	Immunoglobuline isotype / clone status	IgG / rabbit, polyclonal
	Catalog no. / provider	203676 / Abcam
	Demasking of antigen	N/A
	Blocking	3%H_2O_2 in Methanol, NHS S-2012[2], 2.5%
	Dilution and incubation parameters	1:500, room temperature, 30 min
	Secondary antibody used	HaR IgG BA-1100[2], 1:200

Table 1 (cont.)

Type I collagen	Immunoglobuline isotype / clone status	IgG1 / mouse, monoclonal
	Catalog no. / provider	C2456 / Sigma-Aldrich (St. Louis, MO, United States)
	Demasking of antigen	Protease XIV and Hyaluronidase
	Blocking	Bloxall SP-6000[2], NHS S-2000[2], 1:20
	Dilution and incubation parameters	1:2000, room temperature, 30 minutes
	Secondary antibody used	HaM IgG BA-2000[2], 1:200
Type II collagen	Immunoglobuline isotype / clone status	MIgG2A kappa light chain / mouse, monoclonal
	Catalog no. / provider	CIIC1 / DSHB[a]
	Demasking of antigen	Protease XIV and Hyaluronidase
	Blocking	Bloxall SP-6000[2], NHS S-2000[2], 1:20
	Dilution and incubation parameters	1:6, room temperature, 30 minutes
	Secondary antibody used	HaM IgG BA-2000[2], 1:200
Type III collagen	Immunoglobuline isotype / clone status	FH-7AIgG1 / mouse, monoclonal
	Catalog no. / provider	C 7805 / Sigma-Aldrich (St. Louis, MO, United States)
	Demasking of antigen	ProteaseXIV and Hyaluronidase
	Blocking	
	Dilution and incubation parameters	1:4000, room temperature, 30 minutes
	Secondary antibody used	HaM IgG BA-2000[2], 1:200
Type IV collagen	Immunoglobuline isotype / clone status	MIgG1 kappa light chain / mouse, monoclonal
	Catalog no. / provider	M3F7 / DSHB[a]
	Demasking of antigen	N/A
	Blocking	Bloxall SP-6000[2]
	Dilution and incubation parameters	1:5, room temperature, 30 minutes
	Secondary antibody used	HaM IgG BA-2000[2], 1:200

The photomicrographs shown in Figure 2 were produced by digital photography using an automated scanning microscopy workstation, consisting of a M2 AxioImager microscope (Zeiss, Goettingen, Germany), 40 × Plan-Apochromate objective [numerical aperture (N.A.) = 0.95; Zeiss)], two-axis computer controlled stepping motor system (4"× 3" XY; Prior Scientific, Jena, Germany), focus encoder (Heidenhain, Traunreut, Germany) and color digital camera (AxioCam MRc; 2/3" CCD sensor, 1388 × 1040 pixels; Zeiss). The whole system was controlled by the software Stereo Investigator (Version 11.06.2; MBF Bioscience, Williston, VT, United States). Approximately 600 three-dimensional (3D) images with 25 image planes and distance of 1 µm between the image planes were captured for the composite in each Figure 2A, 2C, 2H and 2J. These images were made into one montage each using the Virtual Slide module of the StereoInvestigator software; the size of the resulting 3D virtual slides varied between 1.9 GB and 6.6 GB. The high-power photomicrographs shown in Figure 2D-G, 2I and 2K were created from the virtual slides using the software Biolucida Viewer (Version 2019.3.4; MBF Bioscience).

Figure 3 was produced using a Zeiss Axiophot Microscope equipped with an Axiocam HRc digital camera (2/3" CCD sensor, 1388 × 1040 pixels; Zeiss) that was controlled by the software Zeiss Axiovision SE64 (Rel. 4.9.1 SP2). The images were taken in transmitted light mode without (Figure 3A) or with polarized light (Figure 3B) using a Zeiss Plan-Neofluar 5x objective (N.A. = 0.15). The polarized image was taken in black and white mode of the digital camera. Illumination was adjusted using the automatic measurement function of the Zeiss Axiovision software.

Figures 4-15 were produced as Figure 2. On average approximately 850 3D images with 25 image planes and distance of 1 µm between the image planes were captured for the composite in each Panels A in Figures 4-15; the size of the resulting 3D virtual slides varied between 1.7 GB and 9.4 GB. Panels B-G in Figures 4-15 were also created from the virtual slides using the software Biolucida Viewer (Version 2019.3.4; MBF Bioscience).

The final figures were constructed using Corel Photo-Paint X7 and Corel Draw X7 (both versions 20.1.0.708; Corel, Ottawa, Canada). Only adjustments of contrast and brightness were made using Corel Photo-Paint, without altering the appearance of the original materials.

Bonar scores were determined on all Panels B-G in Figures 4-15 (collagen arrangement was only assessed on Figure 4 (Azan trichrome stain) and Figure 10 (immunohistochemical detection of type I collagen). Furthermore, cell counting was performed using the StereoInvestigator software on all virtual slides. All cells (except for cells inside micovessels) were counted at the position of regions B-G in Figures 4-15, representing 45000 µm^2 each. In case of Azan trichrome stain and immunohistochemical detection of type I collagen, type III collagen and type IV collagen all cells were counted, whereas in case of CD34, CD68, Ki-67, laminin, MMP-2, MMP-9, tenomodulin and type I procollagen only immunopositive cells were counted.

Sections from the first part of the biopsy showed the following (due to the complexity of the results of the various investigations their specific interpretation is provided next to each finding, together with references to the relevant literature):

Azan trichrome staining demonstrated that this part of the biopsy mostly consisted of a region with elongated fibroblast-like cells (tenocytes) arranged in long and parallel chains between collagen fibers (Figure 2A and B).

Type 1 collagen is the most abundant collagen of the human body, present in tendons, ligaments, organ capsules and scar tissue, *etc*.[21]. Immunohistochemical detection of type I collagen (Figure 2C-G and 3A) revealed five different regions within this part of the biopsy, characterized by (1) Organized, slightly undulating type I collagen and high cell density (Figure 2D and "1" in Figure 3A) (this region represented most of the area of the section); (2) Organized type I collagen with discernible crimp arrangement and a few cells (Figure 2E and "2" in Figure 3A); (3) Organized type I collagen with discernible crimp arrangement and almost complete absence of cells (Figure 2F and "3" in Figure 3A); (4) Almost complete absence of immunolabeling for type I collagen and a few, rounded cells (Figure 2G and "4" in Figure 3A) and (5) almost complete absence of immunolabeling for type I collagen but a high cell density ("5" in Figure 3A).

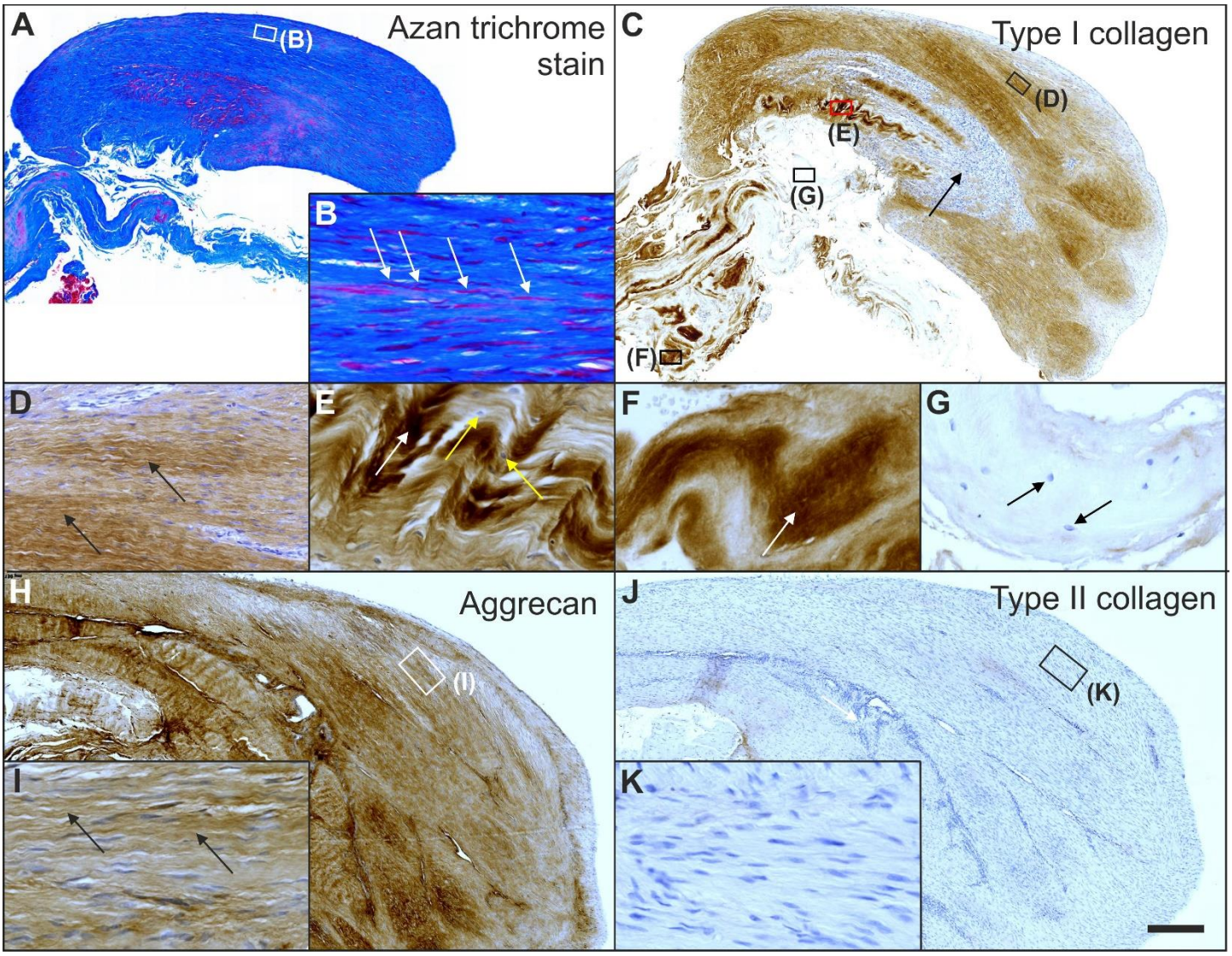

Figure 2 Histological and immunohistochemical analysis of representative sections from the first part of the biopsy that was investigated in this study. A and B: Section stained with Azan trichrome stain; cells are in red and collagen is in blue (inset in Panel A, position of the high-power photomicrograph displayed in Panel B; white arrows in Panel B, elongated, fibroblast-like cells (tenocytes) arranged in long and parallel chains between collagen fibers); C-G: Immunohistochemical detection of type I collagen in a section adjacent to the one shown in Panel A; counterstaining was performed with Mayer's hematoxylin (black arrow in Panel C, region with almost complete absence of immunolabeling for type I collagen but a high cell density; insets in Panel C, position of the high-power photomicrographs displayed in Panels D-G, showing the following four different regions: D: Immunolabeling for organized, slightly undulating type I collagen (black arrows in Panel D) and high cell density; E: Immunolabeling for organized type I collagen with discernible crimp arrangement (white arrow in Panel E) and a few cells (yellow arrows in Panel E); F: Immunolabeling for organized type I collagen with discernible crimp arrangement (white arrow in Panel F) and absence of cells; G: Absence of immunolabeling for type I collagen and a few, rounded cells (black arrows in Panel G); H and I: Immunohistochemical detection of aggrecan in a section adjacent to the ones

shown in Panels A and C of the same biopsy; counterstaining was performed with Mayer's hematoxylin (inset in Panel H, position of the high-power photomicrograph displayed in Panel I; black arrows in Panel I, immunolabeling for aggrecan); J and K: Immunohistochemical detection of type II collagen in another section adjacent to the ones shown in Panels A, C and H of the same biopsy; counterstaining was also performed with Mayer's hematoxylin (inset in Panel J, position of the high-power photomicrograph displayed in Panel K). The scale bar in Panel J represents 250 µm in Panels A, C, H, J and 50 µm in Panels B, D-G, I, K.

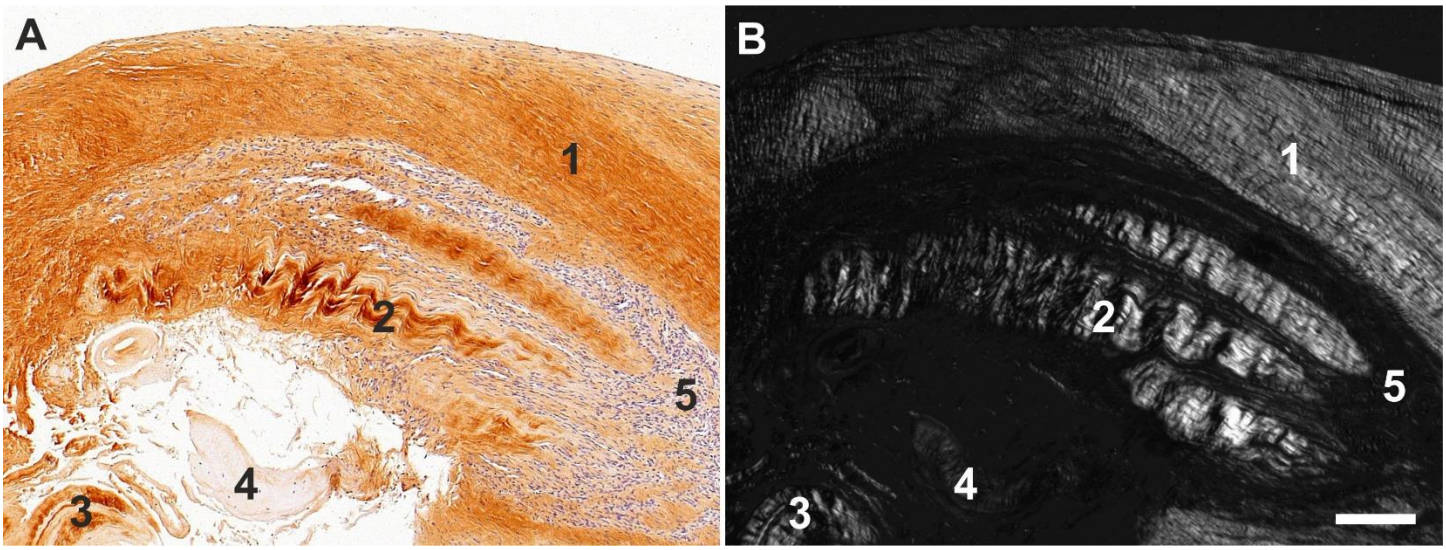

Figure 3 Histological and immunohistochemical analysis of a representative section from the first part of the biopsy that was investigated in this study. A: Immunohistochemical detection of type I collagen, showing the following five different regions (high-power photomicrographs are provided in Figure 2): [1] Organized, slightly undulating type I collagen and high cell density; [2] Organized type I collagen with discernible crimp arrangement and a few cells; [3] Organized type I collagen with discernible crimp arrangement and almost complete absence of cells; [4] Almost complete absence of immunolabeling for type I collagen and a few, rounded cells; and [5] Almost complete absence of immunolabeling for type I collagen but a high cell density; B: Corresponding polarized light microscopic image of the same field of view. Note the clear difference in collagen fiber birefringence between regions 1 and 2, and the absence of collagen fiber birefringence in regions 4 and 5. The scale bar represents 200 µm in Panels A and B.

Additional immunohistochemical analysis showed immunolabeling for aggrecan (Figure 2H and I) but not for type II collagen (Figure 2J and K). Aggrecan and type II collagen are markers of tissues with a fibrocartilaginous phenotype and thus, intermittent compressive load acting on the tendinous tissue[22]. Specifically, the presence of aggrecan in a tendon increases its capacity to imbibe water and, thus, to withstand compression; type II collagen is the typical collagen found in hyaline and various fibrous cartilages[22].

Collectively, the presence of immunolabeling for type I collagen and aggrecan and the absence of immunolabeling for type II collagen in the region of regenerative tendon tissue indicate that the latter was exposed to intermittent tensile load and probably slight intermittent compressive load, which is characteristic for the supraspinatus tendon (tensile load during contraction of the supraspinatus muscle; slight compressive load during adduction of the arm and wrapping the supraspinatus tendon around the humeral head).

Investigation of the section shown in Figure 3A with polarization microscopy demonstrated a clear difference in collagen fiber birefringence between regions 1 and 2, as well as absence of collagen fiber birefringence in regions 4 and 5 (Figure 3B).

A section from the second part of the biopsy that was stained with Azan trichrome stain also showed regions with elongated fibroblast-like cells arranged in long and parallel chains between collagen fibers (Figure 4A and E-G).

In addition, regions with unorganized collagen with (Figure 4B) or without (Figure 4C) formation of microvessels were found, as well as a spot with very high density of cells and microvessels (Figure 4D). Of note, no formation of any adipocytes was observed, indicating that the differentiation of stem cells (initially derived from adipose tissue) was guided by the new location and microenvironment. In the absence of adipose tissue the cells did not form adipose tissue but apparently followed the signaling coming from the injured tendon.

Based on the findings shown in Figure 4, sections from the second part of the biopsy were exposed to antibodies for the detection of CD34 (Figure 5), type IV collagen (Figure 6), Ki-67 (Figure 7), tenomodulin (Figure 8), type I procollagen (Figure 9), type I collagen (Figure 10), type III collagen (Figure 11), laminin (Figure 12), MMP-2 (Figure 13), MMP-9 (Figure 14) and CD68 (Figure 15), revealing for each of the regions shown in Figure 4A-G a different, complex pattern of immunolabeling (summarized in Table 2). Weakest

immunolabeling was found in the regions with unorganized collagen (Figure 4B and C), whereas strongest immunolabeling was observed in the spot with very high density of cells and microvessels (Figure 4D).

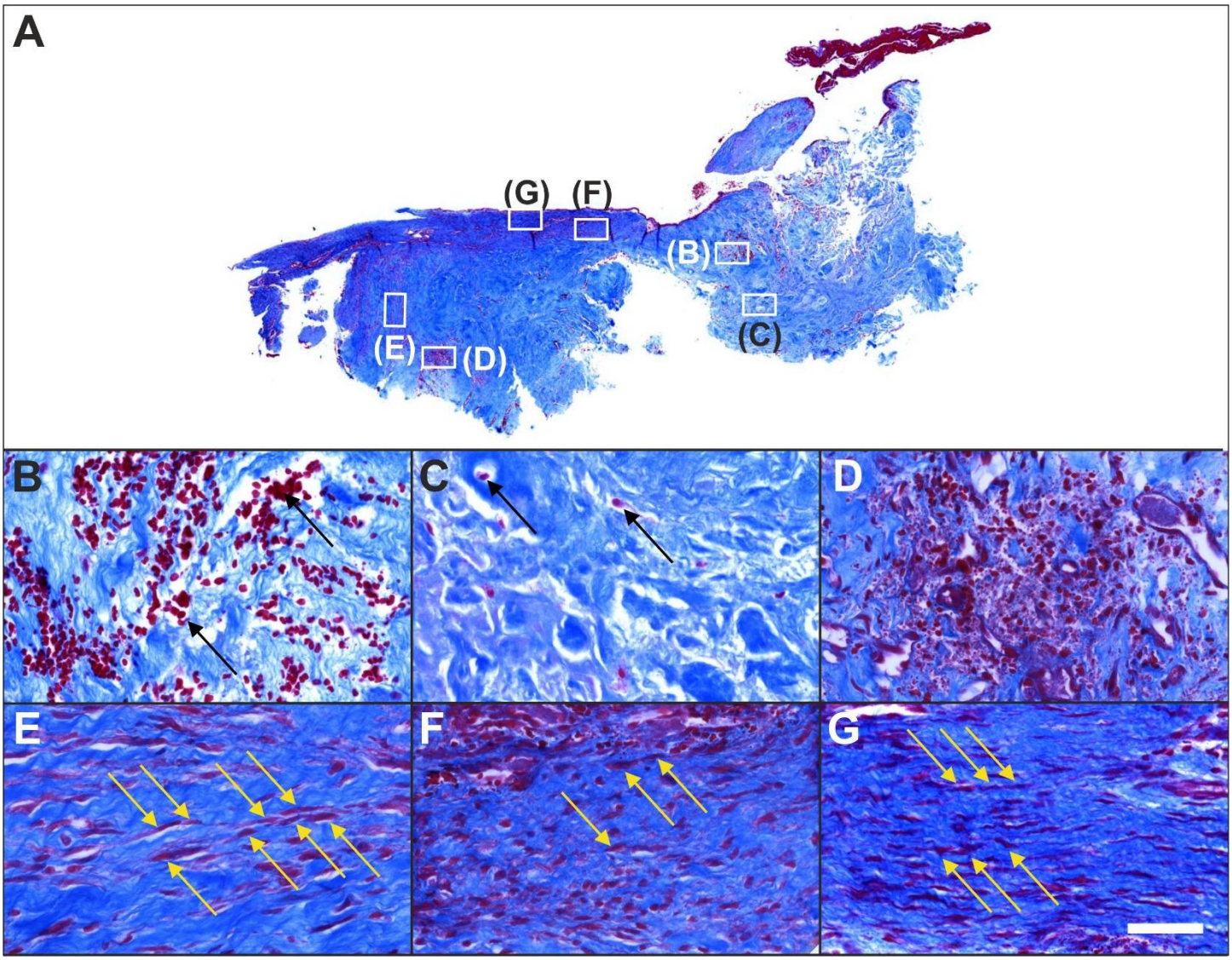

Figure 4 Histological analysis of a representative section of the second part of the biopsy that was investigated in this study (section stained with Azan trichrome stain; cells are in red and collagen is in blue). A: Low-power overview (insets, position of the high-power photomicrographs displayed in Panels B-G); B: Degenerative tendon tissue with formation of microvessels (black arrows, blood cells); C: Degenerative tendon tissue without formation of microvessels (black arrows, rounded cells); D: Spot with very high density of cells and microvessels; E: Tendon tissue in the depth of the biopsy (yellow arrows, elongated, fibroblast-like cells (tenocytes) arranged in long and parallel chains between collagen fibers); F: Tendon tissue below an outer surface of the biopsy (yellow arrows, elongated, fibroblast-like cells (tenocytes) arranged in long and parallel chains between collagen fibers); G: Tendon tissue at an outer surface of the biopsy (yellow arrows, elongated, fibroblast-like cells (tenocytes) arranged in long and parallel chains between collagen fibers). The scale bar in Panel G represents 630 µm in Panel A and 50 µm in Panels B-G.

CD34 is considered a common progenitor cell marker and is expressed by a wide range of cell types, including bone marrow hematopoietic stem cells, MSCs and endothelial progenitor cells[23]. CD34 is primarily expressed by small or newly formed vessels, while endothelial cells of the placenta, lymphatic tissue and larger veins have been reported to be CD34 negative[24,25]. More specifically, CD34 is widely regarded as a marker of vascular endothelial progenitor cells (note that a subset of adult endothelial cells within smaller blood vessels was also reported to be CD34 positive[25]. More than 50% of freshly isolated MSCs express the CD34 cell marker; however, human cultured MSCs are commonly immunonegative for CD34[26]. Accordingly, the presence of CD34+ immunolabeling in endothelial cells of microvessels

in regions D and F of the second part of the investigated biopsy (Figure 5D and F) may indicate ongoing angiogenesis in highly specific regions of the investigated biopsy ten weeks post injection of UA-ADRCs. On the other hand, anti CD34 immunohistochemistry could not be used to assess the potential presence of injected UA-ADRCs and their non-endothelial descendants in the investigated biopsy.

Table 2 Histological and immunohistochemical features of different regions within the second part of the biopsy that was investigated in the present study.

Absence or presence of individual features is coded as – (absence), +/- (minimal presence), + (slight presence), ++ (significant presence) and +++ (overwhelming presence). Column "Figure" indicates the corresponding figures in which detailed documentation is provided. MMP: Matrix metalloproteinase. CD, cluster of differentiation ; MMP, matrix metalloproteinase.

Feature	Region in Figure 4						Figure
	B	C	D	E	F	G	
Presence of microvessels	++	-	+++	+/-	-	-	4
Dense, unorganized cluster of cells and microvessels	-	-	+++	-	-	-	4
Elongated cells in a chain-like arrangement	-	-	-	++	+	+++	4
Immunohistochemical detection of…							
…CD34 in capillary endothelial cells	-	-	++	-	+++	+	5
…Type IV collagen in the basement membrane of microvessels	+	-	+++	+++	+	+	6
…Ki-67 in cells inside microvessel walls	+/-	-	+++	-	-	-	7
…Ki-67 in cells outside microvessel walls	-	+/-	+++	-	+++	-	7
…Intracellular tenomodulin	+	-	+++	+/-	-	-	8
…Extracellular tenomodulin	-	-	+++	-	-	-	8
…Type I procollagen	-	+/-	+++	+++	+++	+	9
…Unorganized type I collagen	+/-	-	+++	+++	-	-	10
…Organized, slightly undulating Type I collagen	-	-	-	+/-	++	+++	10
…Type III collagen	+	+/-	+	+	-	-	11
…Intracellular laminin	+/-	+/-	+++	+++	+	+	12
…Extracellular laminin	-	-	+++	+	-	-	12
…Intracellular MMP-2	+/-	+/-	+++	++	++	+	13
…Extracellular MMP-2	-	-	+++	++	+++	+	13
…Intracellular MMP-9	+/-	+/-	+/-	-	+/-	+/-	14
…Extracellular MMP-9	-	-	-	-	-	-	14
…CD68	+/-	+/-	++	+	+/-	+/-	15

The macromolecular network of type IV collagen provides the scaffold for basement membranes[27]; type IV collagen is the most abundant member of the basement membrane[28]. Thus, immunohistochemical detection of type IV collagen is suitable for detecting vessels in connective tissue independent of endothelial markers. Immunolabeling for type IV collagen was found in the basement membrane of microvessels in all regions the investigated biopsy ten weeks post injection of UA-ADRCs, except for regions in which no microvessels were found (Figure 6). Of note, by immunohistochemical detection of type IV collagen many vessels were found in the degenerative tendon tissue (*i.e.*, those areas that included regions B and C in Figure 4), whereas no immunolabeling for CD34 was found in the degenerative tendon tissue. This finding demonstrates that the majority of endothelial cells in the second part of the biopsy that was investigated in this study was not immunopositive for CD34, which is in line with reports in the literature[24, 25].

Ki-67 is a cellular marker for proliferation[29]. The presence of immunolabeling for Ki-67 in cells inside microvessel walls in region D of the second part of the investigated biopsy (Figure 7D) is in line with the presence of immunolabeling for CD34 in endothelial cells of microvessels in this region (Figure 5D). Furthermore, it appears reasonable to hypothesize that immunolabeling for Ki-67 in cells outside microvessel walls in region D (Figure 7D) could indicate the presence of injected UA-ADRCs and their non-endothelial descendants in this region ten weeks post injection of UA-ADRCs (note that this hypothesis cannot be tested because UA-ADRCs can in principle not be labeled); and immunolabeling for Ki-67 in cells with the characteristic morphology of tenocytes in region F indicates tendon regeneration (Figure 7F).

Tenomodulin is a tendon-specific marker important for tendon maturation, with key implications for residing tendon stem/progenitor cells and the regulation of endothelial cell migration[30-32]. The abundant intracellular and extracellular presence of tenomodulin in region D of the second part of the biopsy (Figure 8D) is in line with the hypothesis that tendon regeneration observed in the investigated biopsy was 'orchestrated' from this region, further supporting the hypothesis that region D in the second part of the investigated biopsy hosted injected UA-ADRCs and their descendants (see also Figure 4D). On the other hand, the presence of tenomoduline immunopositive cells inside microvessels in region B of the second part of the biopsy (Figure 8B) may indicate an unsuccessful attempt of the body to endogenously

initiate tendon regeneration by transferring corresponding cells *via* the blood stream into the injured/degenerative tissue

Type I procollagen is a triple-stranded, rope-like molecule that is processed by enzymes outside the cell, followed by self-arrangement of the processed molecules into long, thin collagen fibrils that cross-link to one another in the extracellular space[33,34]. Accordingly, immunolabeling for type I procollagen in cells outside microvessel walls in region D as well as in regions E and F of the second part of the investigated biopsy (Figure 9D-F) indicate that these regions were involved in tendon regeneration in the investigated biopsy.

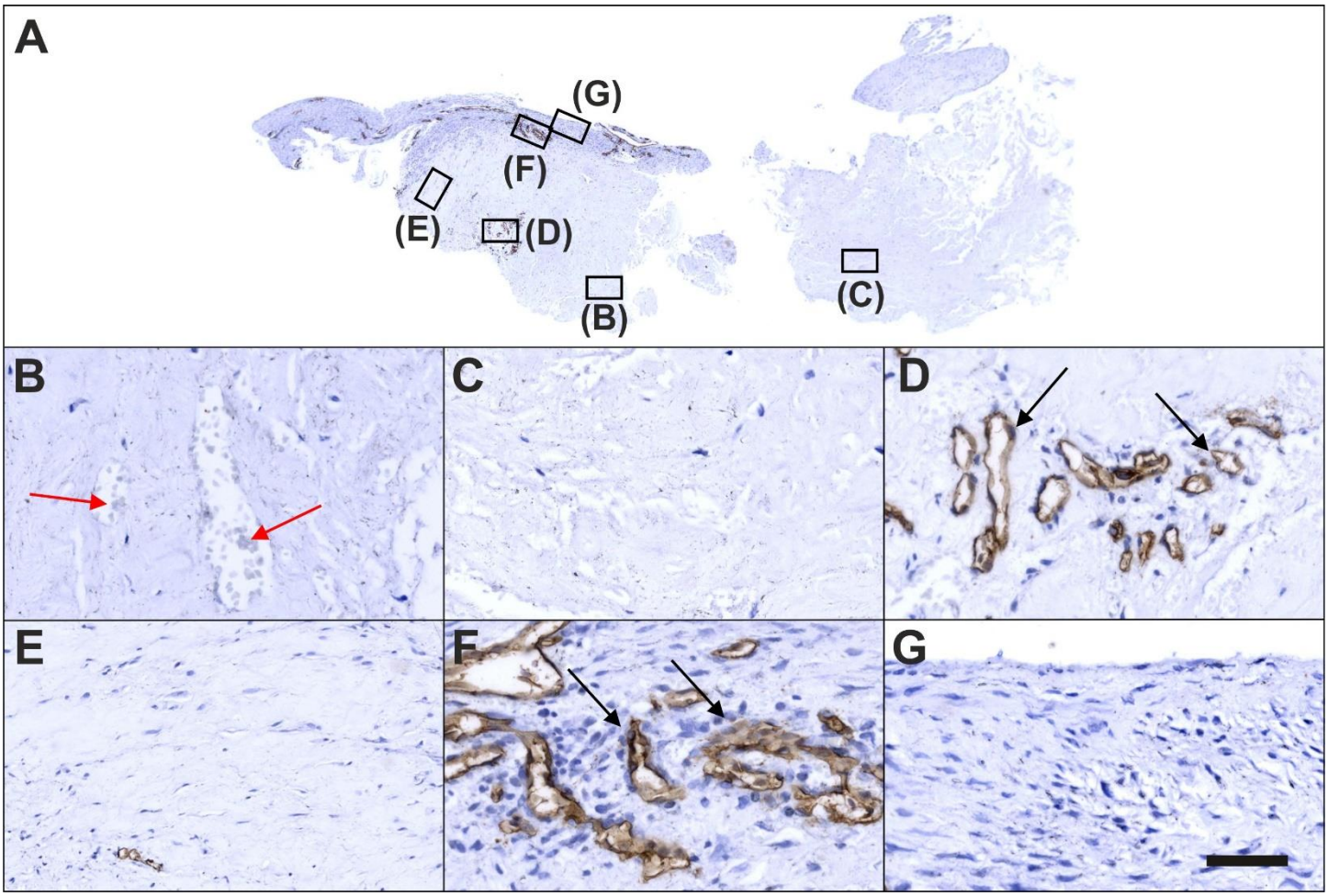

Figure 5 Immunohistochemical detection of CD34 in a section of the second part of the biopsy that was investigated in this study (section adjacent to the one shown in Figure 4; counterstaining was performed with Mayer's hematoxylin). A: Low-power overview (insets, position of the high-power photomicrographs displayed in Panels B-G); B: Position of degenerative tendon tissue with formation of microvessels (red arrows, cells inside a microvessel); C: Position of degenerative tendon tissue without formation of microvessels; D: Position of a spot with very high density of cells and microvessels (black arrows, immunolabeling for CD34 in endothelial cells of microvessels); E: Position of tendon tissue in the depth of the biopsy; F: Position of tendon tissue below an outer surface of the biopsy (black arrows, immunolabeling for CD34 in endothelial cells of microvessels); G: Position of tendon tissue at an outer surface of the biopsy. The scale bar in Panel G represents 630 µm in Panel A and 50 µm in Panels B-G. CD, cluster of cluster of differentiation.

The finding of unorganized Type I collagen found in regions D and E as well as of slightly undulating Type I collagen in regions F and G of the second part of the investigated biopsy (Figure 10D-E) indicates that these regions as well were involved in tendon regeneration, with region G representing fully regenerated tendon tissue.

Unorganized type III collagen is present in scar tissue and is considered representing higher hardness but lower strength than organized type I collagen[35,36]. Type III collagen was found in the degenerative tissue but not the regenerative tissue in the second part of the investigated biopsy (Figure 11). Of note, the patterns of type I procollagen and type I collagen detection (Figures 9 and 10) were inverse compared to the pattern of type III collagen detection (Figure 11). This finding indicated that treatment of sPTRCT with injection of UA-ADRCs may result in histological regeneration without scar formation.

Preprints (www.preprints.org) | NOT PEER-REVIEWED | Posted: 28 June 2021 doi:10.20944/preprints202009.0532.v2

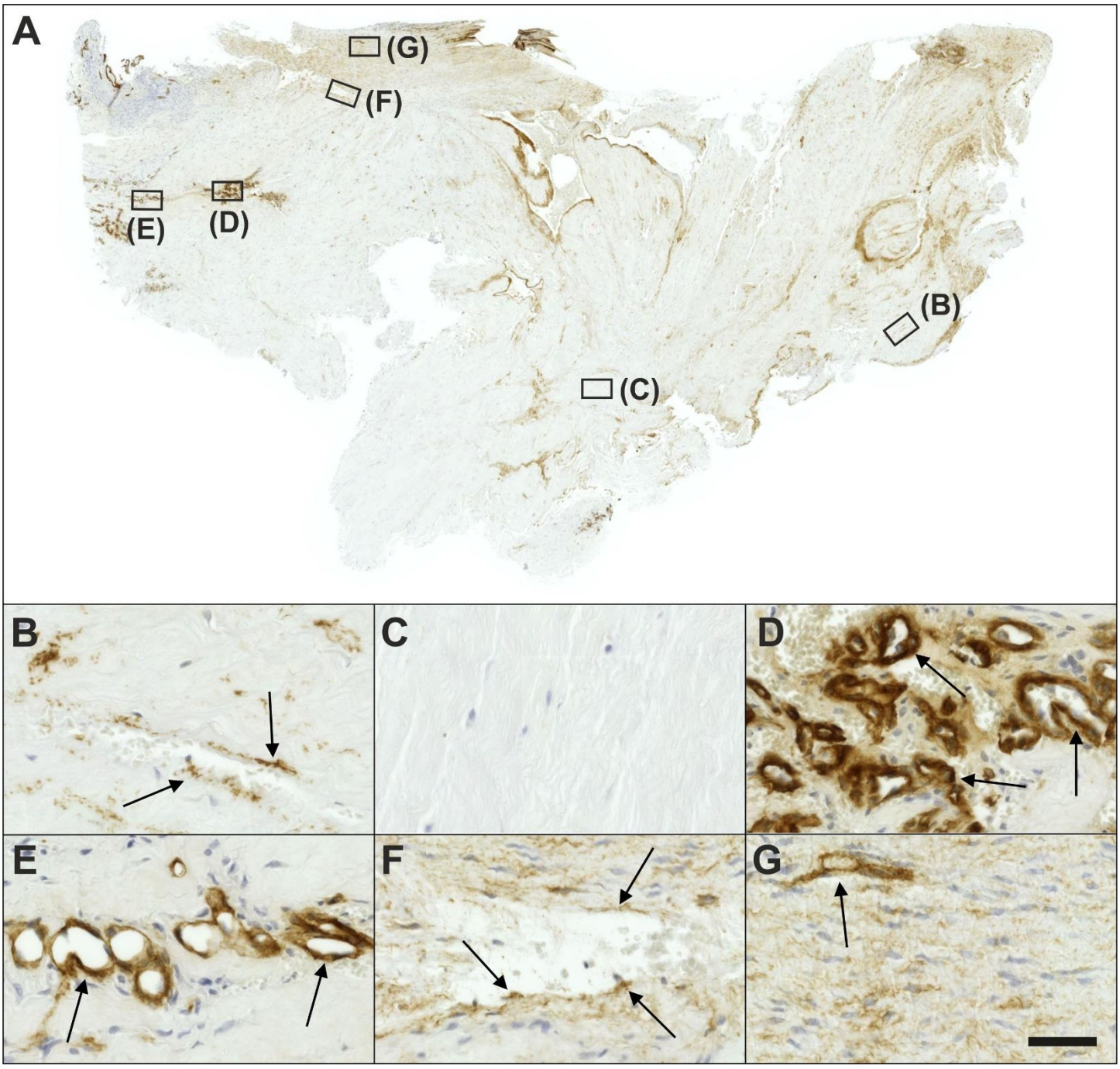

Figure 6 Immunohistochemical detection of type IV collagen in a section of the second part of the biopsy that was investigated in this study (section adjacent to the one shown in Figure 4; counterstaining was performed with Mayer's hematoxylin). A: Low-power overview (insets, position of the high-power photomicrographs displayed in Panels B-G); B: Position of degenerative tendon tissue with formation of microvessels (black arrows, immunolabeling for type IV collagen in the basement membrane of microvessels); C: position of degenerative tendon tissue without formation of microvessels; D: Position of a spot with very high density of cells and microvessels (black arrows, immunolabeling for type IV collagen in the basement membrane of microvessels); E: Position of tendon tissue in the depth of the biopsy (black arrows, immunolabeling for type IV collagen in the basement membrane of microvessels); F: Position of tendon tissue below an outer surface of the biopsy (black arrows, immunolabeling for type IV collagen in the basement membrane of microvessels); G: Position of tendon tissue at an outer surface of the biopsy (black arrow, immunolabeling for type IV collagen in the basement membrane of microvessels). The scale bar in Panel G represents 630 µm in Panel A and 50 µm in Panels B-G.

Preprints (www.preprints.org) | NOT PEER-REVIEWED | Posted: 28 June 2021 doi:10.20944/preprints202009.0532.v2

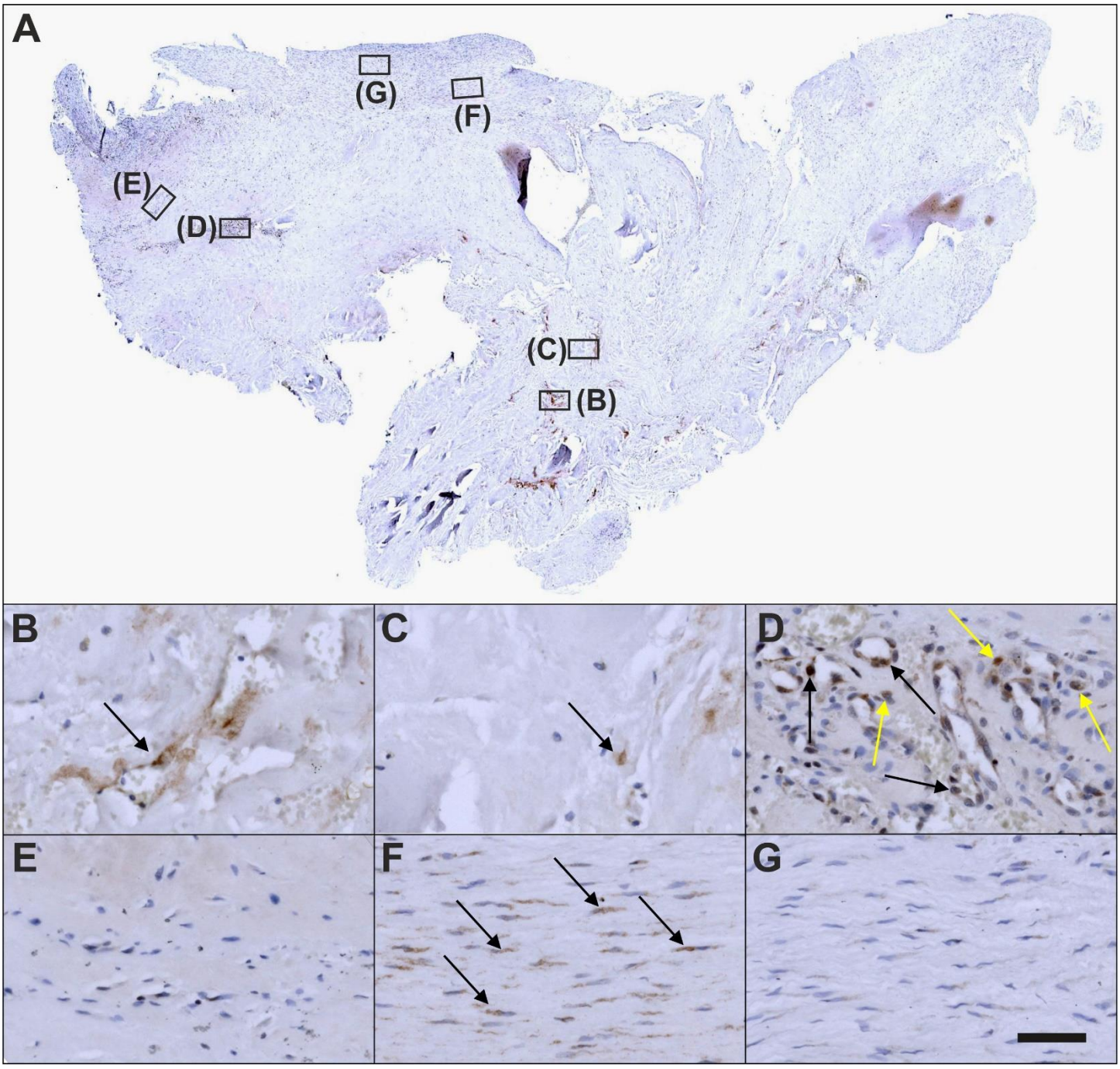

Figure 7 Immunohistochemical detection of Ki-67 in a section of the second part of the biopsy that was investigated in this study (section adjacent to the one shown in Figure 4; counterstaining was performed with Mayer's hematoxylin). A: Low-power overview (insets, position of the high-power photomicrographs displayed in Panels B-G); B: Position of degenerative tendon tissue with formation of microvessels (black arrow, intracellular immunolabeling for Ki-67); C: Position of degenerative tendon tissue without formation of microvessels (black arrow, intracellular immunolabeling for Ki-67); D: Position of a spot with very high density of cells and microvessels (black arrows, intracellular immunolabeling for Ki-67 inside microvessel walls; yellow arrows, intracellular immunolabeling for Ki-67 outside microvessel walls); E: Position of tendon tissue in the depth of the biopsy; F: Position of tendon tissue below an outer surface of the biopsy (black arrows, intracellular immunolabeling for Ki-67 in elongated cells in a chain-like arrangement); G: Position of tendon tissue at an outer surface of the biopsy. The scale bar in Panel G represents 630 µm in Panel A and 50 µm in Panels B-G.

Preprints (www.preprints.org) | NOT PEER-REVIEWED | Posted: 28 June 2021 doi:10.20944/preprints202009.0532.v2

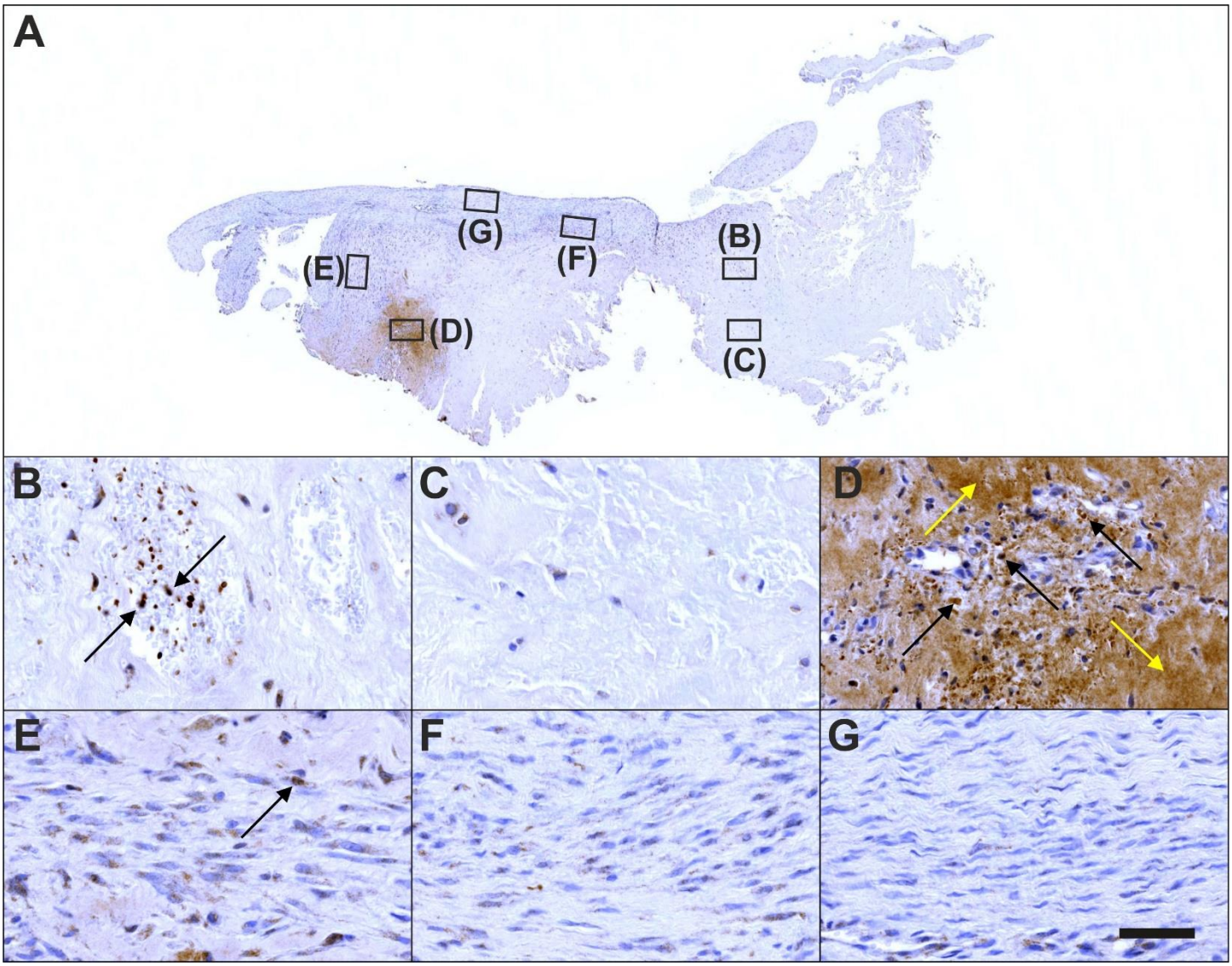

Figure 8 Immunohistochemical detection of tenomodulin in a section of the second part of the biopsy that was investigated in this study (section adjacent to the one shown in Figure 4; counterstaining was performed with Mayer's hematoxylin). A: Low-power overview (insets, position of the high-power photomicrographs displayed in Panels B-G); B: Position of degenerative tendon tissue with formation of microvessels (black arrows, intracellular immunolabeling for tenomodulin in cells inside microvessels); C: Position of degenerative tendon tissue without formation of microvessels; D: Position of a spot with very high density of cells and microvessels (black arrows, intracellular immunolabeling for tenomodulin; yellow arrows, extracellular immunolabeling for tenomodulin); E: Position of tendon tissue in the depth of the biopsy (black arrows, intracellular immunolabeling for tenomodulin); F: Position of tendon tissue below an outer surface of the biopsy; G: Position of tendon tissue at an outer surface of the biopsy. The scale bar in Panel G represents 630 µm in Panel A and 50 µm in Panels B-G.

Laminin is an essential component of the extracellular matrix in soft tissues and modulates a number of cellular functions, including adhesion, differentiation and migration[37]. An *in vitro* study on mouse embryonic stem cell migration found that laminin decreased cell aggregation and increased migration[38]. Another *in vitro* study on tenocytes isolated from injured rotator cuff tendons of human patients concluded that an early increase in the expression of laminin could be beneficial to tendon healing by expediting cellular migration, attachment and growth[39]. Thus, the presence of intracellular and extracellular immunolabeling for laminin in regions D and E of the second part of the investigated biopsy (Figure 12D and E) are in line with the hypothesis that precursors of endothelial cells and tenocytes migrated from region D (where they were generated) *via* region E to region F where tendon regeneration took place.

The interstitial collagenase MMP-2 catalyzes cleavage of collagen fibrils and soluble native type I collagen[40]. A number of recent studies demonstrated that MMP-2 plays an important role in proliferation, migration and angiogenesis of

MSCs[41]. Thus, the presence of intracellular and extracellular immunolabeling for MMP-2 in regions D-F of the second part of the investigated biopsy (Figure 13D-F) is in line with the hypothesis that precursors of endothelial cells and tenocytes migrated from region D (where they were generated) *via* region E to region F where tendon regeneration took place. Of note, MMP-2 was also positively associated with adipogenic and chondrogenic differentiation of MSCs[42], which was not observed in this study. This was most probably due to the fact that the corresponding studies were performed *in vitro* with single (or only a few) stimulating and inhibiting markers, whereas *in vivo* under the conditions of tissue injury the fate of MSCs depends on constant induction of differentiation and re-confirmation by complex signals released and communicated from the local microenvironment[43,44].

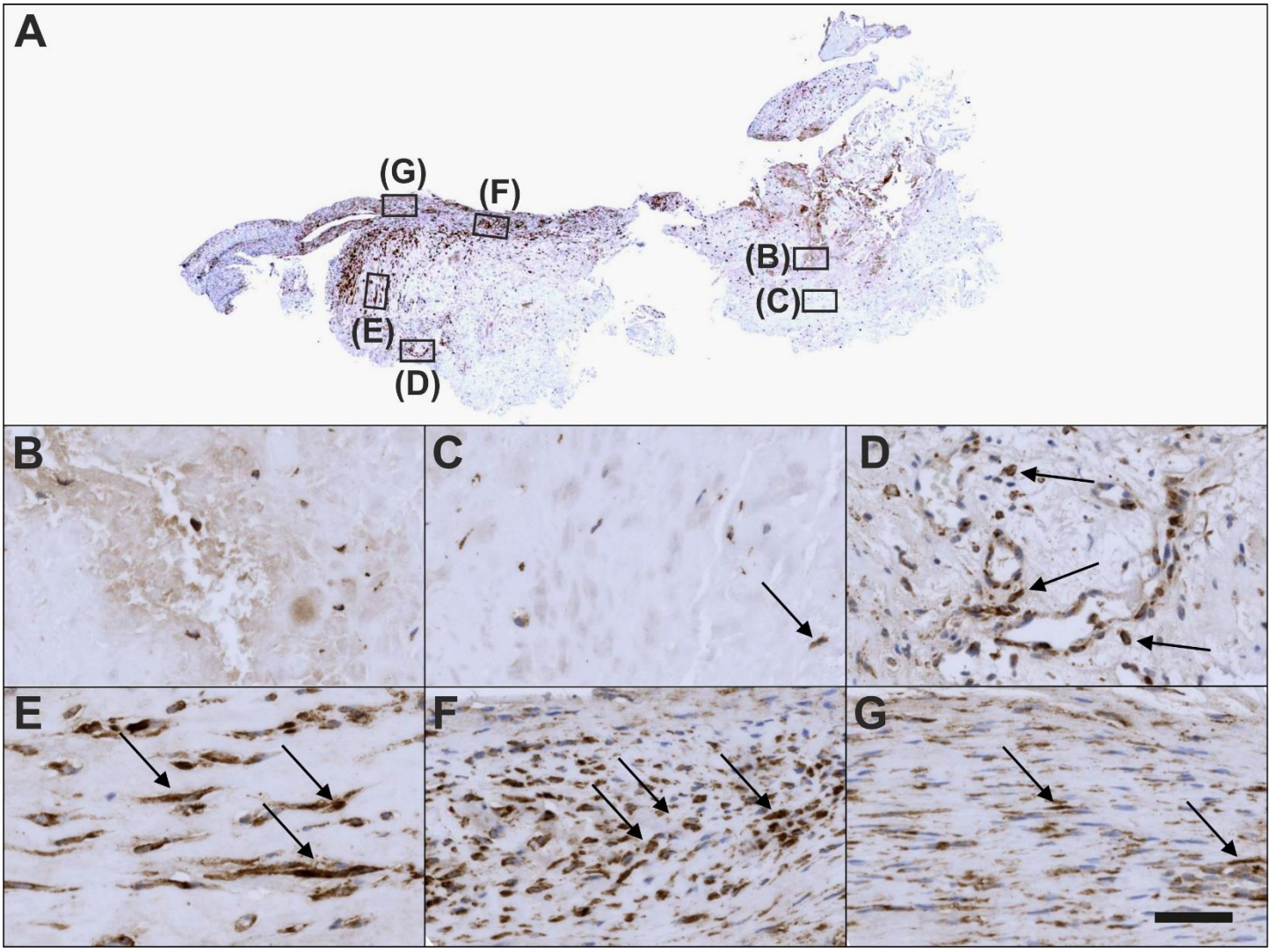

Figure 9 Immunohistochemical detection of type I procollagen in a section of the second part of the biopsy that was investigated in this study (section adjacent to the one shown in Figure 4; counterstaining was performed with Mayer's hematoxylin). A: Low-power overview (insets, position of the high-power photomicrographs displayed in Panels B-G); B: Position of degenerative tendon tissue with formation of microvessels. C: Position of degenerative tendon tissue without formation of microvessels (black arrow, intracellular immunolabeling for type I procollagen); D: Position of a spot with very high density of cells and microvessels (black arrows, intracellular immunolabeling for type I procollagen outside microvessels); E: Position of tendon tissue in the depth of the biopsy (black arrows, intracellular immunolabeling for type I procollagen); F: Position of tendon tissue below an outer surface of the biopsy (black arrows, intracellular immunolabeling for type I procollagen); G: Position of tendon tissue at an outer surface of the biopsy (black arrows, intracellular immunolabeling for type I procollagen). The scale bar in Panel G represents 630 µm in Panel A and 50 µm in Panels B-G.

Preprints (www.preprints.org) | NOT PEER-REVIEWED | Posted: 28 June 2021 doi:10.20944/preprints202009.0532.v2

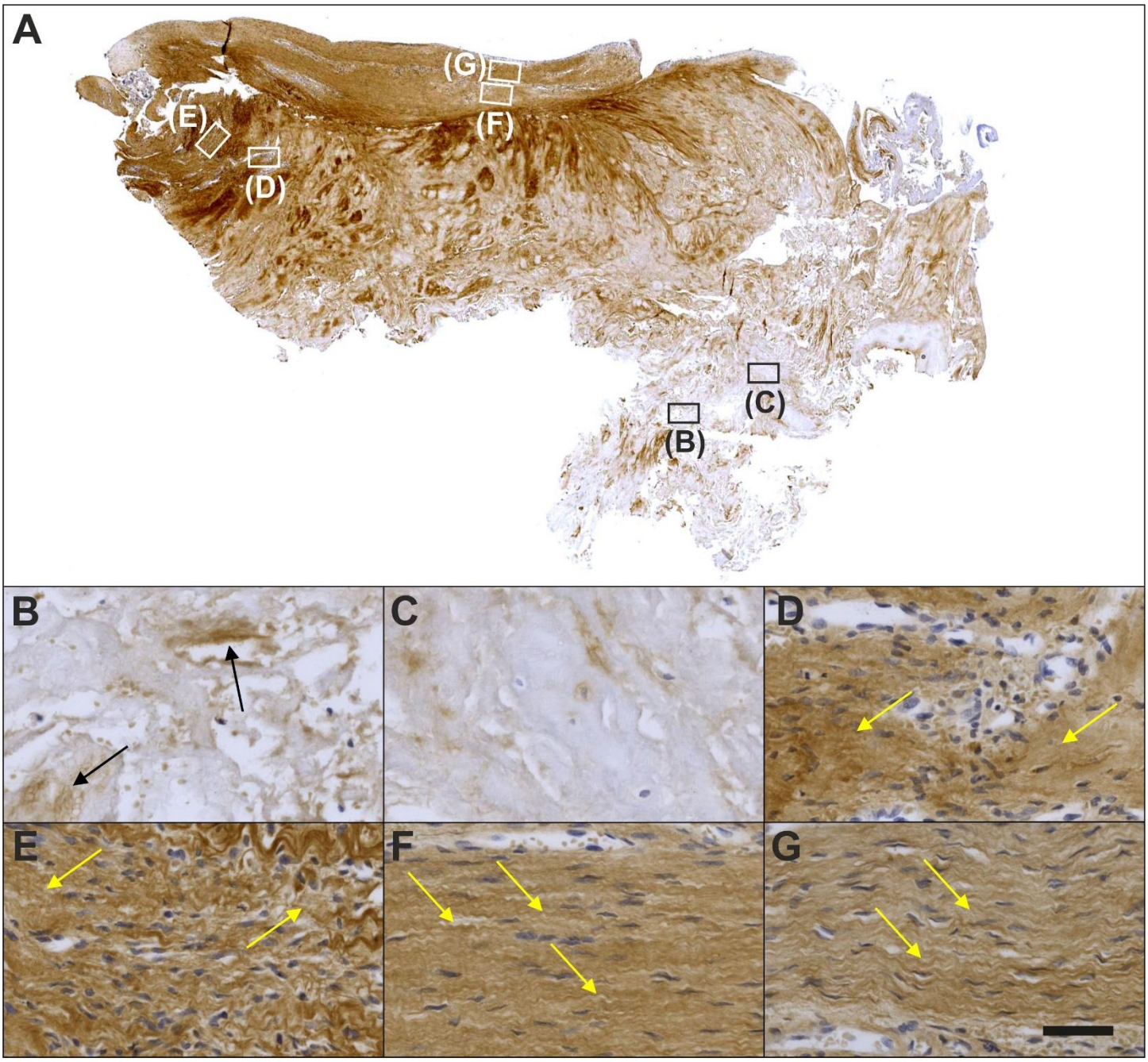

Figure 10 Immunohistochemical detection of type I collagen in a section of the second part of the biopsy that was investigated in this study (section adjacent to the one shown in Figure 4; counterstaining was performed with Mayer's hematoxylin). A: Low-power overview (insets, position of the high-power photomicrographs displayed in Panels B-G); B: Position of degenerative tendon tissue with formation of microvessels (black arrows, immunolabeling for unorganized type I collagen); C: Position of degenerative tendon tissue without formation of microvessels; D: Position of a spot with very high density of cells and microvessels (yellow arrows, immunolabeling for unorganized type I collagen); E: Position of tendon tissue in the depth of the biopsy (yellow arrows, immunolabeling for unorganized type I collagen); F: Position of tendon tissue below an outer surface of the biopsy (yellow arrows, immunolabeling for organized, slightly undulating type I collagen); G: Position of tendon tissue at an outer surface of the biopsy (yellow arrows, immunolabeling for organized, slightly undulating type I collagen). The scale bar in Panel G represents 630 µm in Panel A and 50 µm in Panels B-G.

Preprints (www.preprints.org) | NOT PEER-REVIEWED | Posted: 28 June 2021 doi:10.20944/preprints202009.0532.v2

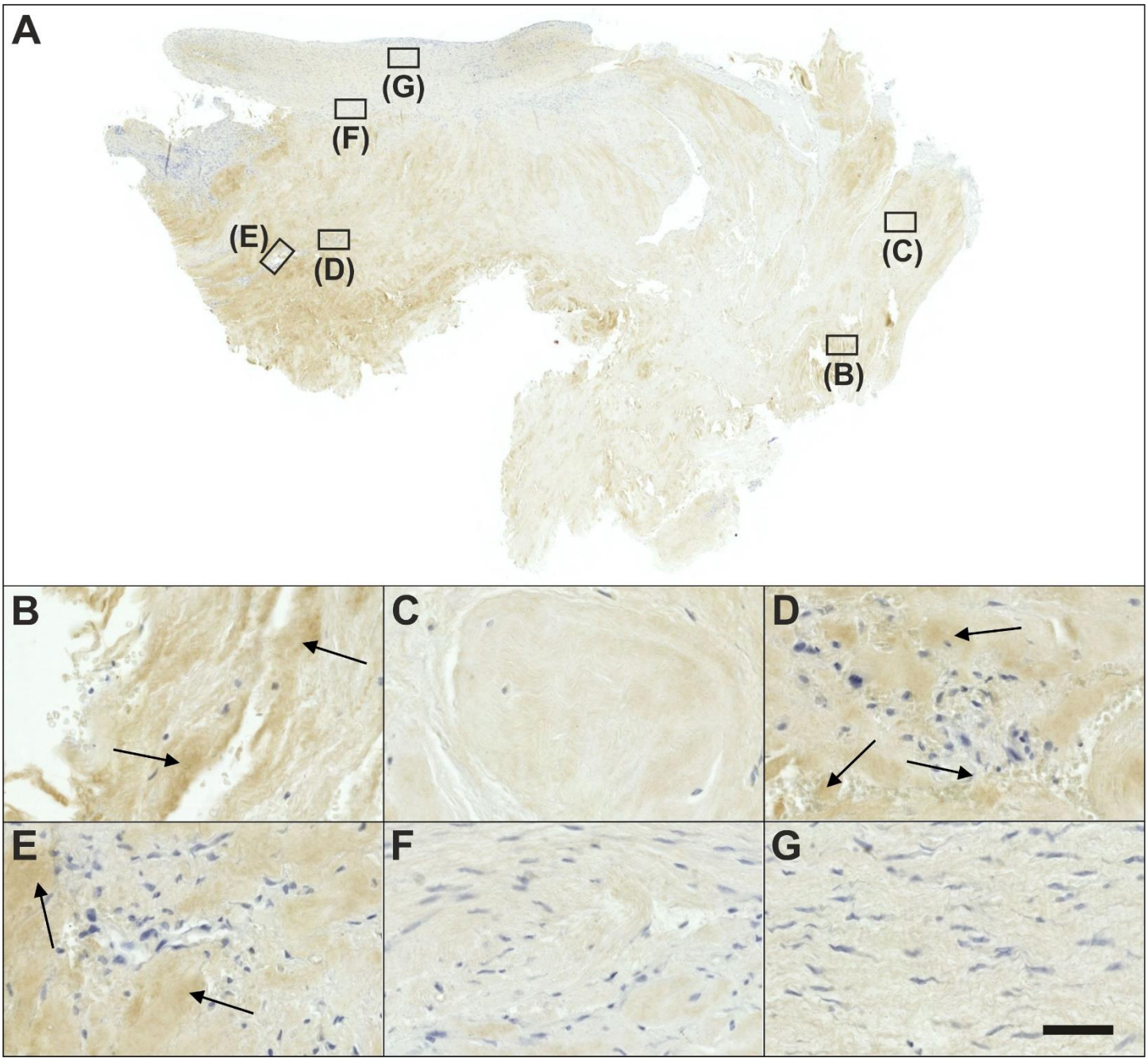

Figure 11 Immunohistochemical detection of type III collagen in a section of the second part of the biopsy that was investigated in this study (section adjacent to the one shown in Figure 4; counterstaining was performed with Mayer's hematoxylin). A: Low-power overview (insets, position of the high-power photomicrographs displayed in Panels B-G); B: Position of degenerative tendon tissue with formation of microvessels (black arrows, extracellular immunolabeling for type III collagen); C: Position of degenerative tendon tissue without formation of microvessels; D: Position of a spot with very high density of cells and microvessels (black arrows, extracellular immunolabeling for type III collagen); E: Position of tendon tissue in the depth of the biopsy (black arrows, extracellular immunolabeling for type III collagen); F: Position of tendon tissue below an outer surface of the biopsy; G: Position of tendon tissue at an outer surface of the biopsy. The scale bar in Panel G represents 630 µm in Panel A and 50 µm in Panels B-G.

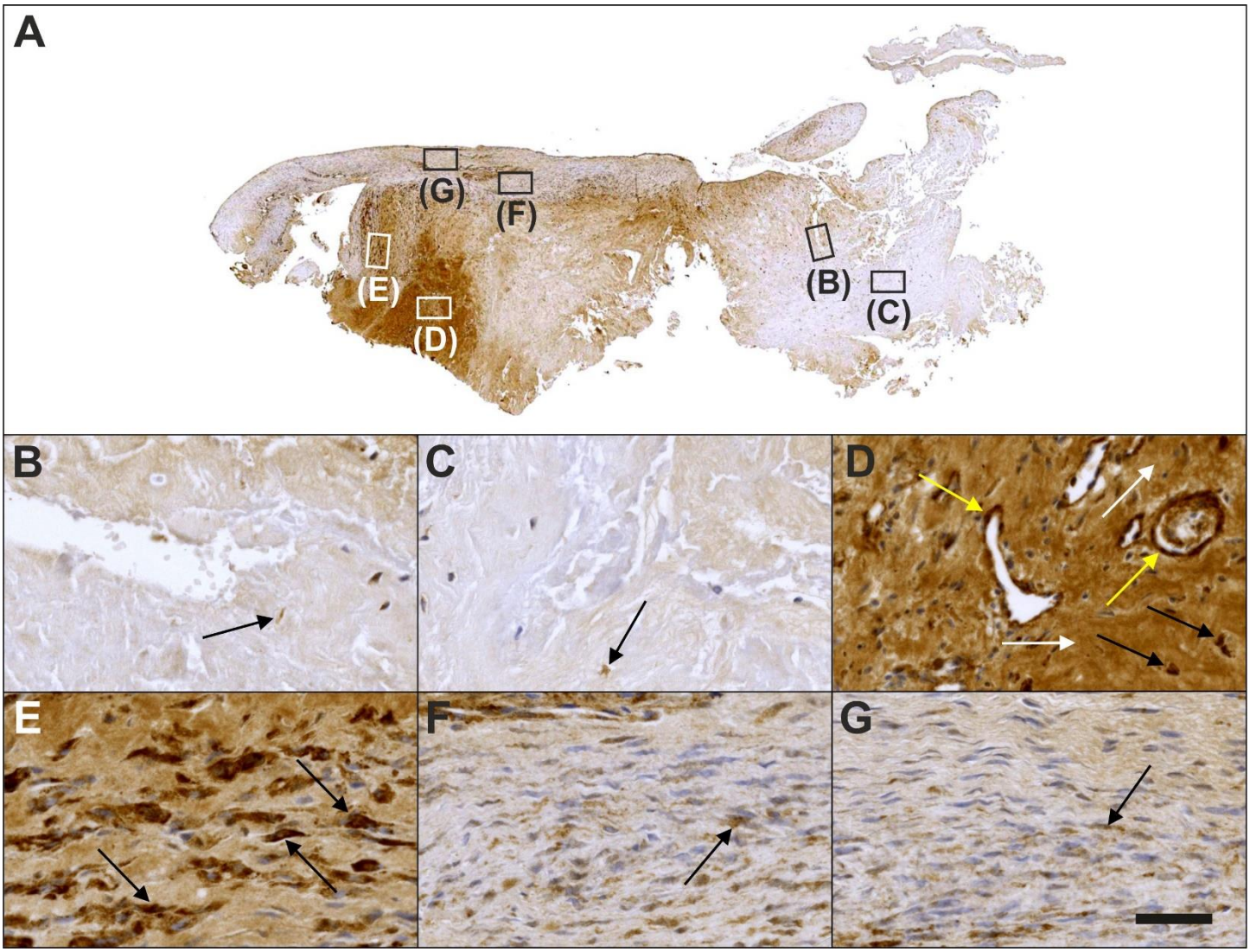

Figure 12 Immunohistochemical detection of laminin in a section of the second part of the biopsy that was investigated in this study (section adjacent to the one shown in Figure 4; counterstaining was performed with Mayer's hematoxylin). A: Low-power overview (insets, position of the high-power photomicrographs displayed in Panels B-G); B: Position of degenerative tendon tissue with formation of microvessels (black arrow, intracellular immunolabeling for laminin); C: Position of degenerative tendon tissue without formation of microvessels (black arrow, intracellular immunolabeling for laminin); D: Position of a spot with very high density of cells and microvessels (black arrows, intracellular immunolabeling for laminin outside microvessel walls; yellow arrows, intracellular immunolabeling for laminin inside microvessel walls; white arrows, extracellular immunolabeling for laminin); E: Position of tendon tissue in the depth of the biopsy (black arrows, intracellular immunolabeling for laminin); F: Position of tendon tissue below an outer surface of the biopsy (black arrow, intracellular immunolabeling for laminin); G: Position of tendon tissue at an outer surface of the biopsy (black arrow, intracellular immunolabeling for laminin). The scale bar in Panel G represents 630 µm in Panel A and 50 µm in Panels B-G.

A recent study suggested that in tendons, MMP-9 is specifically involved in debridement of individual collagen fibrils following tendon overload injury, and prior to deposition of new collagen[45]. This is in line with an earlier study that demonstrated that MMP-9 is involved in tissue degradation during the early phase of healing, whereas MMP-2 contributes to tissue degradation and later remodeling[46]. Another recent study on tenocyte-like cells isolated from biopsies of torn supraspinatus tendons from donors undergoing arthroscopic or open shoulder surgery found an approximately 20000 times higher mean relative mRNA level of MMP-2 than of MMP-9[47]. However, neither individual nor average time intervals between occurrence/diagnosis of tendon tear and surgery were reported in this study[47]. Collectively, these data can explain why almost no MMP-9 immunolabeling was found in the second part of the investigated biopsy (Figure 14).

CD68 is highly expressed by circulating macrophages and tissue macrophages[48]. By producing a variety of growth factors (including IGF-1, VEGF-α, TGF-β and Wnt proteins)

that regulate, among others, differentiation of stem and tissue progenitor cells, proliferation of endothelial cells, activation of myofibroblasts and angiogenesis, macrophages play an important role in regulating tissue regeneration following injury[48]. Thus, the presence of CD68 immunopositive cells particularly in region D (and, to a lesser extent, in region E) of the second part of the investigated biopsy (Figure 15D and E) support the hypothesis that region D represented the site of injection of UA-ADRCs from where tendon regeneration began and was orchestrated.

Bonar scores and results of cell counting are summarized in Tables 3 and 4.

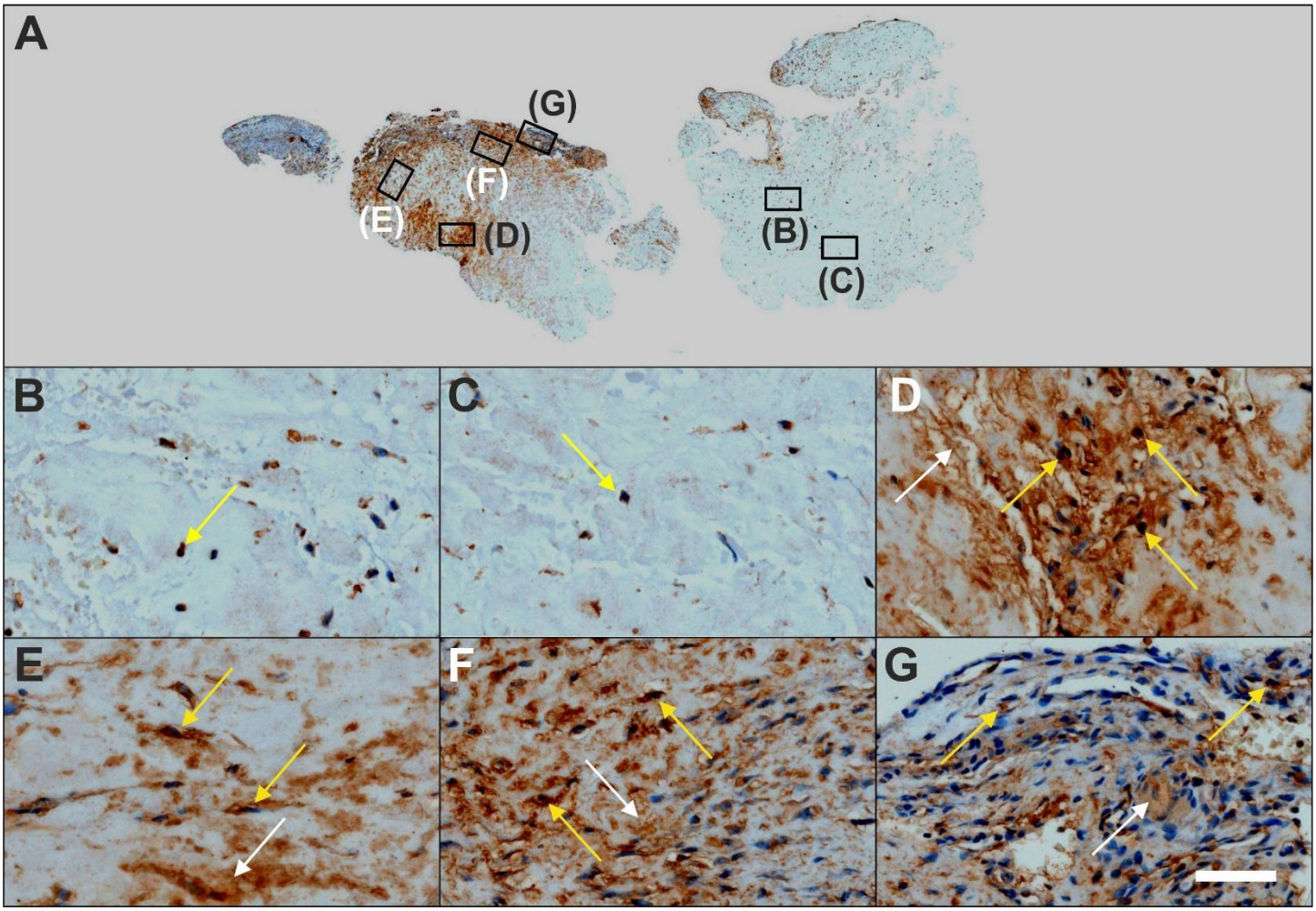

Figure 13 Immunohistochemical detection of matrix metalloproteinase 2 (MMP-2) in a section of the second part of the biopsy that was investigated in this study (section adjacent to the one shown in Figure 4; counterstaining was performed with Mayer's hematoxylin). A: Low-power overview (insets, position of the high-power photomicrographs displayed in Panels B-G); B: Position of degenerative tendon tissue with formation of microvessels (yellow arrow, intracellular immunolabeling for MMP-2); C: Position of degenerative tendon tissue without formation of microvessels (yellow arrow, intracellular immunolabeling for MMP-2); D: Position of a spot with very high density of cells and microvessels (yellow arrows, intracellular immunolabeling for MMP-2; white arrow, extracellular immunolabeling for MMP-2); E: Position of tendon tissue in the depth of the biopsy (yellow arrows, intracellular immunolabeling for MMP-2; white arrow, extracellular immunolabeling for MMP-2); F: Position of tendon tissue below an outer surface of the biopsy (yellow arrows, intracellular immunolabeling for MMP-2; white arrow, extracellular immunolabeling for MMP-2); G: Position of tendon tissue at an outer surface of the biopsy (yellow arrows, intracellular immunolabeling for MMP-2; white arrow, extracellular immunolabeling for MMP-2). The scale bar in Panel G represents 630 µm in Panel A and 50 µm in Panels B-G.

DISCUSSION

To our knowledge this is the very first report demonstrating true regenerative healing of a partial-thickness tear in a human tendon following injection of UA-ADRCs. This is evidenced by comprehensive histological and immunohistochemical analysis of the biopsy taken from this tendon ten weeks post stem cell treatment.

With respect to the latter, the morphological appearance of regions 3 and 4 in Figure 3 and regions B and C in Figures 4-15 is in line with descriptions of the morphological appearance of degenerative supraspinatus tendon tissue at various degrees

in the literature[49-51]. Additionally, to our knowledge, spots within tendons with morphological appearance and immunohistochemical characterization as the one observed in the second part of the biopsy (Panels D in Figures 4-15) have not previously been described in the scientific literature. Besides this, in both parts of the biopsy the morphological appearance of those regions is characterized by elongated fibroblast-like cells arranged in long and parallel chains between collagen fibers (Figure 2B; Panels E-G in Figures 4-15). Organized, slightly undulating type I collagen (region 1 in Figure 3) is consistent with descriptions of the morphological appearance of a process that is known as "regenerative healing in tendons without scar formation" in the literature[52-54]. Of note, this process does not occur in spontaneous tendon healing which typically results in a localized scar defect adjacent to intact enthesis[52,53,55]. Rather, regenerative healing without scar formation so far has been attributed to fetal tendons[52-54].

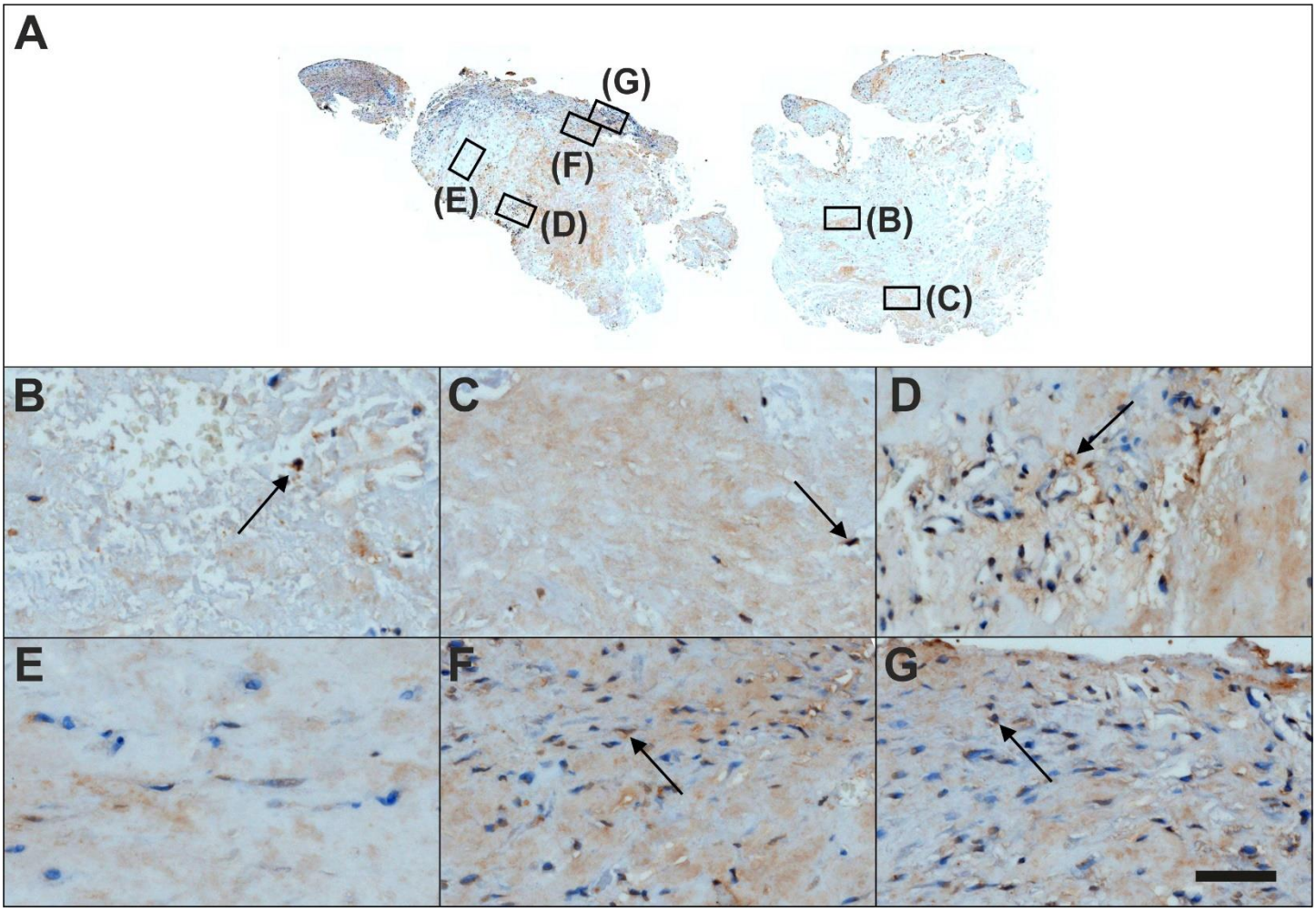

Figure 14 Immunohistochemical detection of matrix metalloproteinase 9 (MMP-9) in a section of the second part of the biopsy that was investigated in this study (section adjacent to the one shown in Figure 4; counterstaining was performed with Mayer's hematoxylin). A: Low-power overview (insets, position of the high-power photomicrographs displayed in Panels B-G); B: Position of degenerative tendon tissue with formation of microvessels (black arrow, intracellular immunolabeling for MMP-9); C: Position of degenerative tendon tissue without formation of microvessels (black arrow, intracellular immunolabeling for MMP-9); D: Position of a spot with very high density of cells and microvessels (black arrow, intracellular immunolabeling for MMP-9); E: Position of tendon tissue in the depth of the biopsy; F: Position of tendon tissue below an outer surface of the biopsy (black arrow, intracellular immunolabeling for MMP-9); G: Position of tendon tissue at an outer surface of the biopsy (black arrow, intracellular immunolabeling for MMP-9). The scale bar in Panel G represents 630 µm in Panel A and 50 µm in Panels B-G.

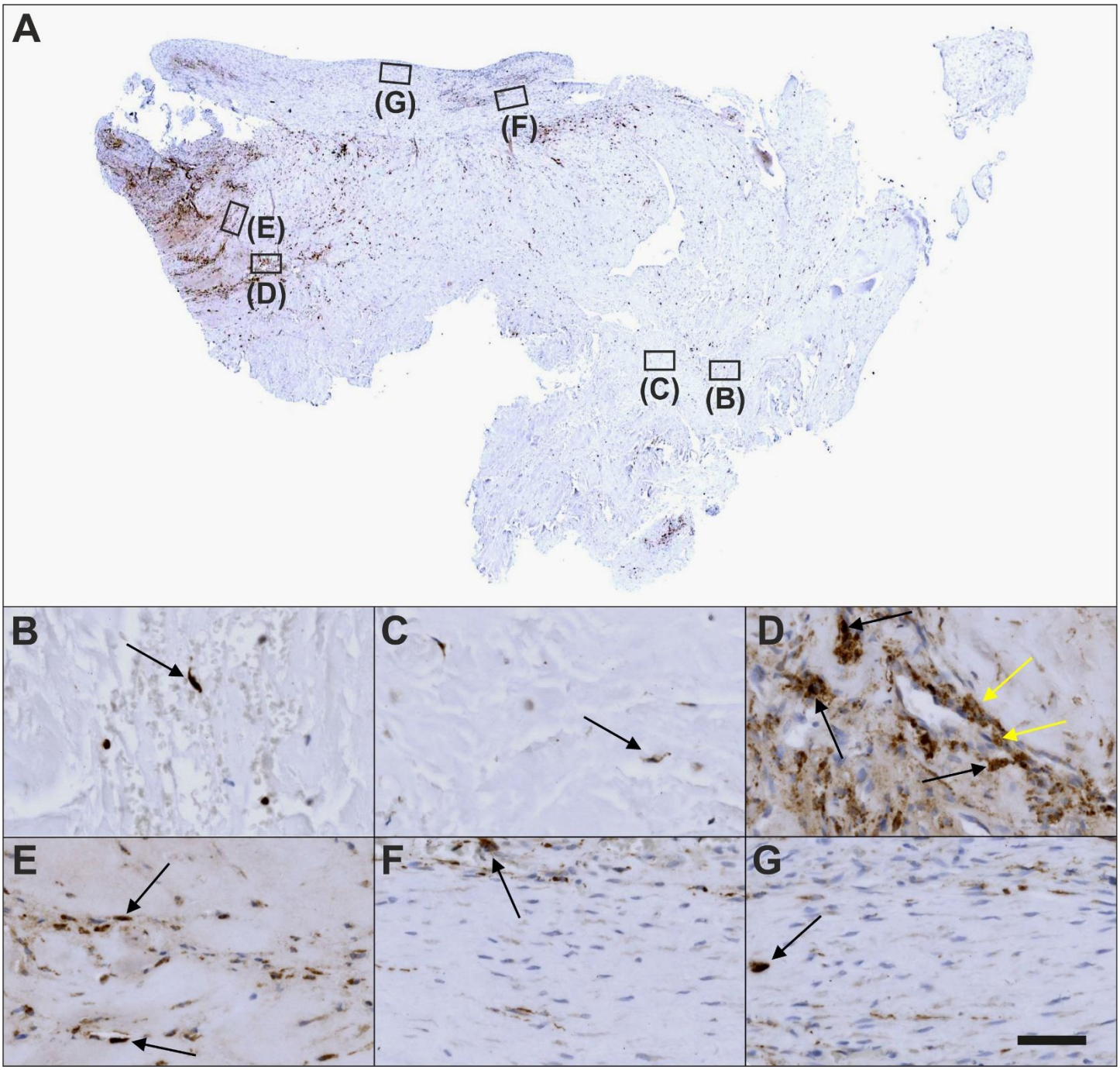

Figure 15 Immunohistochemical detection of CD68 in a section of the second part of the biopsy that was investigated in this study (section adjacent to the one shown in Figure 4; counterstaining was performed with Mayer's hematoxylin). A: Low-power overview (insets, position of the high-power photomicrographs displayed in Panels B-G); B: Position of degenerative tendon tissue with formation of microvessels (black arrow, intracellular labeling for CD68); C: Position of degenerative tendon tissue without formation of microvessels (black arrow, intracellular labeling for CD68); D: Position of a spot with very high density of cells and microvessels (black arrows, intracellular labeling for CD68 outside microvessel walls; yellow arrows, intracellular immunolabeling for CD68 inside microvessel walls); E: Position of tendon tissue in the depth of the biopsy (black arrows, intracellular labeling for CD68); F: Position of tendon tissue below an outer surface of the biopsy (black arrow, intracellular labeling for CD68); G: Position of tendon tissue at an outer surface of the biopsy (black arrow, intracellular labeling for CD68). The scale bar in Panel G represents 630 µm in Panel A and 50 µm in Panels B-G. CD, cluster of cluster of differentiation.

Table 3 Bonar scores of all Regions B-G in Figures 4-15 of the second part of the investigated biopsy.

Note that collagen arrangement was only assessed on sections that showed type I collagen (Azan staining, type I collagen). MMP: Matrix metalloproteinase. CD, cluster of differentiation; MMP, matrix metalloproteinase.

	Azan staining						CD34						Type IV collagen					
	B	**C**	**D**	**E**	**F**	**G**	**B**	**C**	**D**	**E**	**F**	**G**	**B**	**C**	**D**	**E**	**F**	**G**
Cell morphology	3	3	3	2	2	2	2	2	3	2	3	2	3	3	3	1	2	1
Collagen arrangement	3	3	3	1	2	1	-	-	-	-	-	-	-	-	-	-	-	-
Cellularity	1	3	1	1	1	1	3	3	2	2	1	1	1	2	2	1	1	2
Vascularity	3	2	3	1	2	2	0	0	3	1	3	0	2	2	2	2	1	1
Ground substance	0	0	0	0	0	0	1	1	0	0	0	0	0	0	0	0	0	0
	Ki-67						**Tenomodulin**						**Type I procollagen**					
	B	**C**	**D**	**E**	**F**	**G**	**B**	**C**	**D**	**E**	**F**	**G**	**B**	**C**	**D**	**E**	**F**	**G**
Cell morphology	3	3	3	2	1	1	3	3	3	2	2	1	3	3	2	2	2	1
Collagen arrangement	-	-	-	-	-	-	-	-	-	-	-	-	-	-	-	-	-	-
Cellularity	3	3	1	2	2	2	3	3	2	1	1	1	3	3	2	2	1	2
Vascularity	2	1	3	1	0	0	2	2	3	1	1	1	1	1	3	1	1	1
Ground substance	1	1	0	0	0	0	0	0	0	0	0	0	0	0	0	0	0	0
	Type I collagen						**Type III collagen**						**Laminin**					
	B	**C**	**D**	**E**	**F**	**G**	**B**	**C**	**D**	**E**	**F**	**G**	**B**	**C**	**D**	**E**	**F**	**G**
Cell morphology	3	3	3	2	1	1	3	2	3	2	1	1	3	3	3	2	2	2
Collagen arrangement	3	3	2	2	1	2	-	-	-	-	-	-	-	-	-	-	-	-
Cellularity	3	3	1	1	2	1	1	2	1	1	1	1	3	3	2	2	1	1
Vascularity	1	1	2	1	1	1	3	2	3	2	1	1	1	1	3	1	1	1
Ground substance	0	0	0	0	0	0	0	0	0	0	0	0	1	1	0	0	0	0
	MMP-2						**MMP-9**						**CD68**					
	B	**C**	**D**	**E**	**F**	**G**	**B**	**C**	**D**	**E**	**F**	**G**	**B**	**C**	**D**	**E**	**F**	**G**
Cell morphology	3	3	3	2	2	2	3	2	3	3	2	2	3	2	2	2	1	1
Collagen arrangement	-	-	-	-	-	-	-	-	-	-	-	-	-	-	-	-	-	-
Cellularity	2	3	2	2	1	1	3	3	2	2	1	1	3	3	1	2	1	1
Vascularity	2	1	2	1	1	2	1	1	3	1	1	2	2	1	3	2	1	1
Ground substance	1	1	0	0	0	0	1	1	0	0	0	0	1	1	0	0	0	0

Table 4 Number of cells per 45000 µm² area each in all regions B-G in Figures 4-15 of the second part of the investigated biopsy.

Note that in case of Azan trichrome stain and immunohistochemical detection of type I collagen, type III collagen and type IV collagen all cells were counted, whereas in case of CD34, CD68, Ki-67, laminin, matrix metalloproteinase (MMP)-2, MMP-9, tenomodulin and type I procollagen only immunopositive cells were counted. CD, cluster of differentiation; MMP, Matrix metalloproteinase.

Region	**B**	**C**	**D**	**E**	**F**	**G**
Azan staining	64	9	291	150	358	163
CD34	0	0	31	0	58	0
Type IV collagen	11	35	9	8	1	2
Ki-67	10	9	54	0	39	0
Tenomodulin	18	0	20	8	0	0
Type I procollagen	0	3	38	42	109	12
Type I collagen	5	5	121	116	82	78
Type III collagen	33	2	42	7	1	0
Laminin	8	4	30	50	11	13
MMP2	15	6	29	21	21	12
MMP9	3	3	22	0	12	14
CD68	4	3	28	14	4	3

The Bonar score is a well-established scoring system to classify the histopathological findings of tendinopathy and tendon degeneration, focusing on cell morphology, collagen arrangement, cellularity, vascularity and ground substance (Grade 0-Grade 4 each)[56-58]. Bonar scores determined on regions B and C (and, to a lesser extent, region E) indicated substantial tendon degeneration (Table 3), which was in line with the detailed immunohistochemical analysis of the investigated biopsy. On the other hand, Bonar scores determined on regions D, F and G would also have indicated tendon degeneration (or tendinopathy, respectively), despite the fact that these regions showed different aspects of histological regeneration of injured human tendon tissue. In addition, Bonar scores did not adequately reflect the substantial differences in cell numbers among different regions that were found by cell counting (Table 4). Accordingly, the Bonar score appears unsuitable for

characterizing histological regeneration of injured human tendons after injection of UA-ADRCs.

In animal models, injections of adult stem cells isolated from adipose tissue into pathologic tendon tissue has produced a positive biological response[59-63]. Reported beneficial effects include a decreased number of inflammatory cells, improved regeneration of tendons with less scarred healing, improved collagen fiber arrangement, higher load-to-failure and higher tensile strength of the treated tendons[59-63]. These findings support the results we obtained by investigating a biopsy of a human tendon ten weeks post injection of UA-ADRCs. Our comprehensive immunohistochemical analysis of the biopsy with a broad number of antibodies (Tables 1 and 2) allow the conclusion that region D in the second part of the biopsy (Panels D in Figures 4-15) represented the site of injection of UA-ADRCs from where tendon regeneration started. It further indicates that endothelial precursors and tenocytes might have migrated from region D (where they were generated) *via* region E to region F, in which tendon regeneration took place. Induction of differentiation and re-confirmation were most probably guided by complex signals released and communicated from the local microenvironment[43, 44].

Some authors raised concerns about the use of ADSCs/ADRCs in tendon regeneration due to their assumed "indigenous" preference towards forming adipocytes'[64,65], albeit without reference to corresponding findings in the literature. We did not observe formation of adipocytes in the investigated biopsy. The latter result is in line with an earlier finding of our group clearly demonstrating that UA-ADRCs do not form adipocytes when used for treating chronic myocardial infarction[66]. Furthermore, in guided bone regeneration using UA-ADRCs we found substantially less formation of adipocytes (only 2% with stem cells) than without the use of UA-ADRCs (18%)[67]. Collectively, these findings do not only support the role of the local microenvironment for induction and guidance of differentiation of stem cells in the target tissue, but also underscore the need to exercise caution in drawing incorrect conclusions absent of convincing scientific evidence, or without a correct understanding of stem cell biology.

It should be pointed out again that UA-ADRCs can in principle not be labeled because this would render them modified. In this regard UA-ADRCs fundamentally differ from ADSCs that can be derived from UA-ADRCs by culturing[7]. In contrast to UA-ADRCs, ADSCs can be intracellularly labeled with fluorescent probes, as demonstrated by ourselves[7] and many others. Furthermore, ADRCs have been demonstrated to survive, proliferate and differentiate for a long time in the host tissue (discussed in detail in[7]). Because UA-ADRCs cannot be labeled, it is in principle not possible to provide the same evidence for UA-ADRCs as has be done in the literature for ADCS.

For the sake of completeness it should be mentioned that mesenchymal stem cell-derived exosomes have been shown to promote tendon regeneration by facilitating the proliferation and migration of endogenous tendon stem and progenitor cells[68-70]. Thus, one cannot exclude that paracrine effects may play a certain role in histological regeneration of injured human tendon tissue after injection of UA-ADRCs. On the other hand, the latter would only limit the significance of our results if histological regeneration of injured human tendon tissue after injection of UA-ADRCs would be fully due to paracrine effects (only in this case one could replace injection of UA-ADRCs by injection of exosomes or secretomes of mesenchymal stem cells). However, there is no evidence in the literature supporting this view. In this regard a recent systematic review[71] summarized five studies in which the potential of stem cells conditioned medium (secretome) in ligament and tendon healing was investigated. Of note, in none of these studies injection of stem cells conditioned medium was compared to injection of UA-ADRCs or ADSCs. In summary, the question about potential contribution of paracrine effects to the histological regeneration of injured human tendon tissue after injection of UA-ADRCs as described in this study cannot be answered at this time. Clarifying the role of paracrine effects in tendon repair after injection of UA-ADRCs would require controlled trials with repeated taking of biopsies. This may be achieved in animal studies in the future.

Conclusions of this study are presented on the basis of a single time point analysis of molecular and cellular events. As such, limitations consist in the fact that only a single patient was investigated; no control biopsy was analyzed, and the scientists who analyzed the biopsy were not blinded. It further was not the aim of the present study to establish a clinical treatment. To more conclusively evaluate clinical results with UA-ADRCs for incomplete tendon tears, a respective pivotal RCT is now recruiting[72], which is based on the encouraging clinical results of the pilot study[72].

CONCLUSION

In summary, the results of this study indicate, for the first time, that treatment of an injured human tendon with unmodified, autologous regenerative cells can enable true regenerative healing. This process has previously been attributed only to fetal tendon development. It is of special importance that this success was achieved without prior manipulation, stimulation and/or (genetic) reprogramming of the cells injected.

Acknowledgements

We thank Aschauer B, Haderer A, Harbauer C and Tost S for excellent and highly valuable technical support.

Funding

This study was in part supported by the Alliance of Cardiovascular Researchers (New Orleans, LA, USA), by IsarKlinikum in Munich (Munich, Germany) and by InGeneron, Inc. (Houston, TX, USA). The sponsors of the study did not have any influence on data collection, analysis or publication. No constraints were placed on publication of the data.

Availability of data and materials
The data that support the findings of this study are available from the corresponding author upon reasonable request.

Authors' contributions
Alt EU, Rothoerl R, Hoppert M, Frank HG, Wuerfel T, Alt C and Schmitz C designed the report; Rothoerl R and Hoppert M performed treatment and collected the biopsy; Alt EU, Frank HG, Alt C and Schmitz C collected the patient's clinical data; Alt EU, Frank HG, Wuerfel T, Alt C and Schmitz C analyzed the data and wrote the paper.

Ethics approval and consent to participate
This study is a single self-experiment with the patient's consent. The patient is the first author of this study, Alt E, MD, PhD. Single self-experiments with the patient's unrestricted and free will formation are exempt from approval of an Institutional Review Board in Germany[12]. It was Alt E himself who initiated his own treatment, taking the biopsy and all investigations. Alt E gave informed consent to participate in this study.

Consent for publication
Consent was obtained from the patient for publication of this report and any accompanying images.

Competing interests
Alt EU is Executive Chair of InGeneron, Inc. (Houston, TX) and Chairman of the Board of Isar Klinikum (Munich, Germany). Alt C is managing director of InGeneron GmbH (Munich, Germany) and of SciCoTec (Grünwald, Germany), the principal shareholder of InGeneron, Inc., which owns InGeneron GmbH (Munich, Germany). Schmitz C served as consultant to SciCoTec and the Alliance of Cardiovascular Researchers, and is Advisory Medical Director of InGeneron, Inc.

REFERENCES

1 **Matthewson G**, Beach CJ, Nelson AA, Woodmass JM, Ono Y, Boorman RS, Lo IK, Thornton GM. Partial Thickness Rotator Cuff Tears: Current Concepts. *Adv Orthop* 2015; **2015**: 458786 [PMID: 26171251 DOI: 10.1155/2015/458786]

2 **Coombes BK**, Bisset L, Vicenzino B. Efficacy and safety of corticosteroid injections and other injections for management of tendinopathy: a systematic review of randomised controlled trials. *Lancet* 2010; **376**: 1751-1767 [PMID: 20970844 DOI: 10.1016/S0140-6736(10)61160-9]

3 **Ramírez J**, Pomés I, Cabrera S, Pomés J, Sanmartí R, Cañete JD. Incidence of full-thickness rotator cuff tear after subacromial corticosteroid injection: a 12-week prospective study. *Mod Rheumatol* 2014; **24**: 667-670 [PMID: 24289196 DOI: 10.3109/14397595.2013.857798]

4 **Hurley ET**, Hannon CP, Pauzenberger L, Fat DL, Moran CJ, Mullett H. Nonoperative Treatment of Rotator Cuff Disease With Platelet-Rich Plasma: A Systematic Review of Randomized Controlled Trials. *Arthroscopy* 2019; **35**: 1584-1591 [PMID: 31000394 DOI: 10.1016/j.arthro.2018.10.115]

5 **Schwitzguebel AJ**, Kolo FC, Tirefort J, Kourhani A, Nowak A, Gremeaux V, Saffarini M, Lädermann A. Efficacy of Platelet-Rich Plasma for the Treatment of Interstitial Supraspinatus Tears: A Double-Blinded, Randomized Controlled Trial. *Am J Sports Med* 2019; **47**: 1885-1892 [PMID: 31161947 DOI: 10.1177/0363546519851097]

6 **Kukkonen J**, Joukainen A, Lehtinen J, Mattila KT, Tuominen EK, Kauko T, Aärimaa V. Treatment of non-traumatic rotator cuff tears: A randomised controlled trial with one-year clinical results. *Bone Joint J* 2014; **96-B**: 75-81 [PMID: 24395315 DOI: 10.1302/0301-620X.96B1.32168]

7 **Alt EU**, Winnier G, Haenel A, Rothoerl R, Solakoglu O, Alt C, Schmitz C. Towards a Comprehensive Understanding of UA-ADRCs (Uncultured, Autologous, Fresh, Unmodified, Adipose Derived Regenerative Cells, Isolated at Point of Care) in Regenerative Medicine. *Cells* 2020; **9** [PMID: 32365488 DOI: 10.3390/cells9051097]

8 **Cossu G**, Birchall M, Brown T, De Coppi P, Culme-Seymour E, Gibbon S, Hitchcock J, Mason C, Montgomery J, Morris S, Muntoni F, Napier D, Owji N, Prasad A, Round J, Saprai P, Stilgoe J, Thrasher A, Wilson J. Lancet Commission: Stem cells and regenerative medicine. *Lancet* 2018; **391**: 883-910 [PMID: 28987452 DOI: 10.1016/S0140-6736(17)31366-1]

9 **Bajek A**, Gurtowska N, Gackowska L, Kubiszewska I, Bodnar M, Marszałek A, Januszewski R, Michalkiewicz J, Drewa T. Does the liposuction method influence the phenotypic characteristic of human adipose-derived stem cells? *Biosci Rep* 2015; **35** [PMID: 26182374 DOI: 10.1042/BSR20150067]

10 **Polly SS**, Nichols AEC, Donnini E, Inman DJ, Scott TJ, Apple SM, Werre SR, Dahlgren LA. Adipose-Derived Stromal Vascular Fraction and Cultured Stromal Cells as Trophic Mediators for Tendon Healing. *J Orthop Res* 2019; **37**: 1429-1439 [PMID: 30977556 DOI: 10.1002/jor.24307]

11 **Hurd JL**, Facile TR, Weiss J, Hayes M, Hayes M, Furia JP, Maffulli N, Winnier GE, Alt C, Schmitz C, Alt EU, Lundeen M. Safety and efficacy of treating symptomatic, partial-thickness rotator cuff tears with fresh, uncultured, unmodified, autologous adipose-derived regenerative cells (UA-ADRCs) isolated at the point of care: a prospective, randomized, controlled first-in-human pilot study. *J Orthop Surg Res* 2020; **15**: 122 [PMID: 32238172 DOI: 10.1186/s13018-020-01631-8]

12 **Hanley BP**, Bains W, Church G. Review of Scientific Self-Experimentation: Ethics History, Regulation, Scenarios, and Views Among Ethics Committees and Prominent Scientists. *Rejuvenation Res* 2019; **22**: 31-42 [PMID: 29926769 DOI: 10.1089/rej.2018.2059]

13 **Angst F**, Schwyzer HK, Aeschlimann A, Simmen BR, Goldhahn J. Measures of adult shoulder function: Disabilities of the Arm, Shoulder, and Hand Questionnaire (DASH) and its short version (QuickDASH), Shoulder Pain and Disability Index (SPADI), American Shoulder and Elbow Surgeons (ASES) Society standardized shoulder assessment form, Constant (Murley) Score (CS), Simple Shoulder Test (SST), Oxford Shoulder Score (OSS), Shoulder Disability Questionnaire (SDQ), and Western Ontario Shoulder Instability Index (WOSI). *Arthritis Care Res (Hoboken)* 2011; **63 Suppl 11**: S174-S188 [PMID: 22588743 DOI: 10.1002/acr.20630]

14 **Wylie JD**, Beckmann JT, Granger E, Tashjian RZ. Functional outcomes assessment in shoulder surgery. *World J Orthop* 2014; **5**: 623-633 [PMID: 25405091 DOI: 10.5312/wjo.v5.i5.623]

15 **van Kampen DA**, van den Berg T, van der Woude HJ, Castelein RM, Scholtes VA, Terwee CB, Willems WJ. The diagnostic value of the combination of patient characteristics, history, and clinical shoulder tests for the diagnosis of rotator cuff tear. *J Orthop Surg Res* 2014; **9**: 70 [PMID: 25099359 DOI: 10.1186/s13018-014-0070-y]

16 **Zhang J**, Keenan C, Wang JH. The effects of dexamethasone on human patellar tendon stem cells: implications for dexamethasone treatment of tendon injury. *J Orthop Res* 2013; **31**: 105-110 [PMID: 22886634 DOI: 10.1002/jor.22193]

17 **Ryösä A**, Laimi K, Äärimaa V, Lehtimäki K, Kukkonen J, Saltychev M. Surgery or conservative treatment for rotator cuff tear: a meta-analysis. *Disabil Rehabil* 2017; **39**: 1357-1363 [PMID: 27385156 DOI: 10.1080/09638288.2016.1198431]

18 **Ellera Gomes JL**, da Silva RC, Silla LM, Abreu MR, Pellanda R. Conventional rotator cuff repair complemented by the aid of

mononuclear autologous stem cells. *Knee Surg Sports Traumatol Arthrosc* 2012; **20**: 373-377 [PMID: 21773831 DOI: 10.1007/s00167-011-1607-9]

19 **Hernigou P**, Flouzat Lachaniette CH, Delambre J, Zilber S, Duffiet P, Chevallier N, Rouard H. Biologic augmentation of rotator cuff repair with mesenchymal stem cells during arthroscopy improves healing and prevents further tears: a case-controlled study. *Int Orthop* 2014; **38**: 1811-1818 [PMID: 24913770 DOI: 10.1007/s00264-014-2391-1]

20 **Havlas V**, Kotaška J, Koníček P, Trč T, Konrádová Š, Kočí Z, Syková E. [Use of cultured human autologous bone marrow stem cells in repair of a rotator cuff tear: preliminary results of a safety study]. *Acta Chir Orthop Traumatol Cech* 2015; **82**: 229-234 [PMID: 26317295]

21 **Mescher AL.** Junqueira's basic histology text & atlas. 15th ed. New York City, NY: McGraw-Hill Education, 2018

22 **Benjamin M**, Ralphs JR. Fibrocartilage in tendons and ligaments--an adaptation to compressive load. *J Anat* 1998; **193 (Pt 4)**: 481-494 [PMID: 10029181 DOI: 10.1046/j.1469-7580.1998.19340481.x]

23 **Marvasti TB**, Alibhai FJ, Weisel RD, Li RK. $CD34^+$ Stem Cells: Promising Roles in Cardiac Repair and Regeneration. *Can J Cardiol* 2019; **35**: 1311-1321 [PMID: 31601413 DOI: 10.1016/j.cjca.2019.05.037]

24 **Müller AM**, Hermanns MI, Skrzynski C, Nesslinger M, Müller KM, Kirkpatrick CJ. Expression of the endothelial markers PECAM-1, vWf, and CD34 *in vivo* and in vitro. *Exp Mol Pathol* 2002; **72**: 221-229 [PMID: 12009786 DOI: 10.1006/exmp.2002.2424]

25 **Sidney LE**, Branch MJ, Dunphy SE, Dua HS, Hopkinson A. Concise review: evidence for CD34 as a common marker for diverse progenitors. *Stem Cells* 2014; **32**: 1380-1389 [PMID: 24497003 DOI: 10.1002/stem.1661]

26 **Dominici M**, Le Blanc K, Mueller I, Slaper-Cortenbach I, Marini F, Krause D, Deans R, Keating A, Prockop Dj, Horwitz E. Minimal criteria for defining multipotent mesenchymal stromal cells. The International Society for Cellular Therapy position statement. *Cytotherapy* 2006; **8**: 315-317 [PMID: 16923606 DOI: 10.1080/14653240600855905]

27 **Kühn K**. Basement membrane (type IV) collagen. *Matrix Biol* 1995; **14**: 439-445 [PMID: 7795882 DOI: 10.1016/0945-053x(95)90001-2]

28 **Rhodes JM**, Simons M. The extracellular matrix and blood vessel formation: not just a scaffold. *J Cell Mol Med* 2007; **11**: 176-205 [PMID: 17488472 DOI: 10.1111/j.1582-4934.2007.00031.x]

29 **Scholzen T**, Gerdes J. The Ki-67 protein: from the known and the unknown. *J Cell Physiol* 2000; **182**: 311-322 [PMID: 10653597 DOI: 10.1002/(SICI)1097-4652(200003)182:3<311::AID-JCP1>3.0.CO;2-9]

30 **Shukunami C**, Oshima Y, Hiraki Y. Molecular cloning of tenomodulin, a novel chondromodulin-I related gene. *Biochem Biophys Res Commun* 2001; **280**: 1323-1327 [PMID: 11162673 DOI: 10.1006/bbrc.2001.4271]

31 **Brandau O**, Meindl A, Fässler R, Aszódi A. A novel gene, tendin, is strongly expressed in tendons and ligaments and shows high homology with chondromodulin-I. *Dev Dyn* 2001; **221**: 72-80 [PMID: 11357195 DOI: 10.1002/dvdy.1126]

32 **Dex S**, Lin D, Shukunami C, Docheva D. Tenogenic modulating insider factor: Systematic assessment on the functions of tenomodulin gene. *Gene* 2016; **587**: 1-17 [PMID: 27129941 DOI: 10.1016/j.gene.2016.04.051]

33 **Prockop DJ**, Kivirikko KI, Tuderman L, Guzman NA. The biosynthesis of collagen and its disorders (first of two parts). *N Engl J Med* 1979; **301**: 13-23 [PMID: 449904 DOI: 10.1056/NEJM197907053010104]

34 **Prockop DJ**, Kivirikko KI, Tuderman L, Guzman NA. The biosynthesis of collagen and its disorders (second of two parts). *N Engl J Med* 1979; **301**: 77-85 [PMID: 36559 DOI: 10.1056/NEJM197907123010204]

35 **Clore JN**, Cohen IK, Diegelmann RF. Quantitation of collagen types I and III during wound healing in rat skin. *Proc Soc Exp Biol Med* 1979; **161**: 337-340 [PMID: 461460 DOI: 10.3181/00379727-161-40548]

36 **Bhogal RK**, Stoica CM, McGaha TL, Bona CA. Molecular aspects of regulation of collagen gene expression in fibrosis. *J Clin Immunol* 2005; **25**: 592-603 [PMID: 16380822 DOI: 10.1007/s10875-005-7827-3]

37 **Halper J**, Kjaer M. Basic components of connective tissues and extracellular matrix: elastin, fibrillin, fibulins, fibrinogen, fibronectin, laminin, tenascins and thrombospondins. *Adv Exp Med Biol* 2014; **802**: 31-47 [PMID: 24443019 DOI: 10.1007/978-94-007-7893-1_3]

38 **Suh HN**, Han HJ. Laminin regulates mouse embryonic stem cell migration: involvement of Epac1/Rap1 and Rac1/cdc42. *Am J Physiol Cell Physiol* 2010; **298**: C1159-C1169 [PMID: 20089929 DOI: 10.1152/ajpcell.00496.2009]

39 **Molloy TJ**, de Bock CE, Wang Y, Murrell GA. Gene expression changes in SNAP-stimulated and iNOS-transfected tenocytes--expression of extracellular matrix genes and its implications for tendon-healing. *J Orthop Res* 2006; **24**: 1869-1882 [PMID: 16865710 DOI: 10.1002/jor.20237]

40 **Aimes RT**, Quigley JP. Matrix metalloproteinase-2 is an interstitial collagenase. Inhibitor-free enzyme catalyzes the cleavage of collagen fibrils and soluble native type I collagen generating the specific 3/4- and 1/4-length fragments. *J Biol Chem* 1995; **270**: 5872-5876 [PMID: 7890717 DOI: 10.1074/jbc.270.11.5872]

41 **Almalki SG**, Agrawal DK. Effects of matrix metalloproteinases on the fate of mesenchymal stem cells. *Stem Cell Res Ther* 2016; **7**: 129 [PMID: 27612636 DOI: 10.1186/s13287-016-0393-1]

42 **Rezza A**, Sennett R, Rendl M. Adult stem cell niches: cellular and molecular components. *Curr Top Dev Biol* 2014; **107**: 333-372 [PMID: 24439812 DOI: 10.1016/B978-0-12-416022-4.00012-3]

43 **Dong L**, Hao H, Han W, Fu X. The role of the microenvironment on the fate of adult stem cells. *Sci China Life Sci* 2015; **58**: 639-648 [PMID: 25985755 DOI: 10.1007/s11427-015-4865-9]

44 **Wabik A**, Jones PH. Switching roles: the functional plasticity of adult tissue stem cells. *EMBO J* 2015; **34**: 1164-1179 [PMID: 25812989 DOI: 10.15252/embj.201490386]

45 **Baldwin SJ**, Kreplak L, Lee JM. MMP-9 selectively cleaves non-D-banded material on collagen fibrils with discrete plasticity damage in mechanically-overloaded tendon. *J Mech Behav Biomed Mater* 2019; **95**: 67-75 [PMID: 30954916 DOI: 10.1016/j.jmbbm.2019.03.020]

46 **Oshiro W**, Lou J, Xing X, Tu Y, Manske PR. Flexor tendon healing in the rat: a histologic and gene expression study. *J Hand Surg Am* 2003; **28**: 814-823 [PMID: 14507513 DOI: 10.1016/s0363-5023(03)00366-6]

47 **Klatte-Schulz F**, Aleyt T, Pauly S, Geißler S, Gerhardt C, Scheibel M, Wildemann B. Do Matrix Metalloproteases and Tissue Inhibitors of Metalloproteases in Tenocytes of the Rotator Cuff Differ with Varying Donor Characteristics? *Int J Mol Sci* 2015; **16**: 13141-13157 [PMID: 26068238 DOI: 10.3390/ijms160613141]

48 **Vannella KM**, Wynn TA. Mechanisms of Organ Injury and Repair by Macrophages. *Annu Rev Physiol* 2017; **79**: 593-617 [PMID: 27959618 DOI: 10.1146/annurev-physiol-022516-034356]

49 **Hashimoto T**, Nobuhara K, Hamada T. Pathologic evidence of degeneration as a primary cause of rotator cuff tear. *Clin Orthop Relat Res* 2003: 111-120 [PMID: 14612637 DOI: 10.1097/01.blo.0000092974.12414.22]

50 **Lakemeier S**, Reichelt JJ, Patzer T, Fuchs-Winkelmann S, Paletta JR, Schofer MD. The association between retraction of the torn rotator cuff and increasing expression of hypoxia inducible factor 1α and vascular endothelial growth factor expression: an immunohistological study. *BMC Musculoskelet Disord* 2010; **11**: 230 [PMID: 20932296 DOI: 10.1186/1471-2474-11-230]

51 **Ferrer GA**, Miller RM, Yoshida M, Wang JH, Musahl V, Debski RE. Localized Rotator Cuff Tendon Degeneration for Cadaveric Shoulders with and Without Tears Isolated to the Supraspinatus Tendon. *Clin Anat* 2020; **33**: 1007-1013 [PMID: 31750575 DOI: 10.1002/ca.23526]

52 **Beredjiklian PK**, Favata M, Cartmell JS, Flanagan CL, Crombleholme TM, Soslowsky LJ. Regenerative *vs* reparative healing in tendon: a study of biomechanical and histological properties in fetal sheep. *Ann Biomed Eng* 2003; **31**: 1143-1152 [PMID: 14649488 DOI: 10.1114/1.1616931]

53 **Tang QM**, Chen JL, Shen WL, Yin Z, Liu HH, Fang Z, Heng BC, Ouyang HW, Chen X. Fetal and adult fibroblasts display intrinsic differences in tendon tissue engineering and regeneration. *Sci Rep* 2014; **4**: 5515 [PMID: 24992450 DOI: 10.1038/srep05515]

54 **Galatz LM**, Gerstenfeld L, Heber-Katz E, Rodeo SA. Tendon regeneration and scar formation: The concept of scarless healing. *J Orthop Res* 2015; **33**: 823-831 [PMID: 25676657 DOI: 10.1002/jor.22853]

55 **Moser HL**, Doe AP, Meier K, Garnier S, Laudier D, Akiyama H, Zumstein MA, Galatz LM, Huang AH. Genetic lineage tracing of targeted cell populations during enthesis healing. *J Orthop Res* 2018; **36**: 3275-3284 [PMID: 30084210 DOI: 10.1002/jor.24122]

56 **Cook JL**, Feller JA, Bonar SF, Khan KM. Abnormal tenocyte morphology is more prevalent than collagen disruption in asymptomatic athletes' patellar tendons. *J Orthop Res* 2004; **22**: 334-338 [PMID: 15013093 DOI: 10.1016/j.orthres.2003.08.005]

57 **Maffulli N**, Longo UG, Franceschi F, Rabitti C, Denaro V. Movin and Bonar scores assess the same characteristics of tendon histology. *Clin Orthop Relat Res* 2008; **466**: 1605-1611 [PMID: 18437501 DOI: 10.1007/s11999-008-0261-0]

58 **Fearon A**, Dahlstrom JE, Twin J, Cook J, Scott A. The Bonar score revisited: region of evaluation significantly influences the standardized assessment of tendon degeneration. *J Sci Med Sport* 2014; **17**: 346-350 [PMID: 23932935 DOI: 10.1016/j.jsams.2013.07.008]

59 **Kim SH**, Chung SW, Oh JH. Expression of insulin-like growth factor type 1 receptor and myosin heavy chain in rabbit's rotator cuff muscle after injection of adipose-derived stem cell. *Knee Surg Sports Traumatol Arthrosc* 2014; **22**: 2867-2873 [PMID: 23736255 DOI: 10.1007/s00167-013-2560-6]

60 **Valencia Mora M**, Antuña Antuña S, García Arranz M, Carrascal MT, Barco R. Application of adipose tissue-derived stem cells in a rat rotator cuff repair model. *Injury* 2014; **45 Suppl 4**: S22-S27 [PMID: 25384471 DOI: 10.1016/S0020-1383(14)70006-3]

61 **Chen HS**, Su YT, Chan TM, Su YJ, Syu WS, Harn HJ, Lin SZ, Chiu SC. Human adipose-derived stem cells accelerate the restoration of tensile strength of tendon and alleviate the progression of rotator cuff injury in a rat model. *Cell Transplant* 2015; **24**: 509-520 [PMID: 25654771 DOI: 10.3727/096368915X686968]

62 **Gumucio JP**, Flood MD, Roche SM, Sugg KB, Momoh AO, Kosnik PE, Bedi A, Mendias CL. Stromal vascular stem cell treatment decreases muscle fibrosis following chronic rotator cuff tear. *Int Orthop* 2016; **40**: 759-764 [PMID: 26224616 DOI: 10.1007/s00264-015-2937-x]

63 **Tsekes D**, Konstantopoulos G, Khan WS, Rossouw D, Elvey M, Singh J. Use of stem cells and growth factors in rotator cuff tendon repair. *Eur J Orthop Surg Traumatol* 2019; **29**: 747-757 [PMID: 30627922 DOI: 10.1007/s00590-019-02366-x]

64 **Docheva D**, Müller SA, Majewski M, Evans CH. Biologics for tendon repair. *Adv Drug Deliv Rev* 2015; **84**: 222-239 [PMID: 25446135 DOI: 10.1016/j.addr.2014.11.015]

65 **Qi F**, Deng Z, Ma Y, Wang S, Liu C, Lyu F, Wang T, Zheng Q. From the perspective of embryonic tendon development: various cells applied to tendon tissue engineering. *Ann Transl Med* 2020; **8**: 131 [PMID: 32175424 DOI: 10.21037/atm.2019.12.78]

66 **Haenel A**, Ghosn M, Karimi T, Vykoukal J, Shah D, Valderrabano M, Schulz DG, Raizner A, Schmitz C, Alt EU. Unmodified autologous stem cells at point of care for chronic myocardial infarction. *World J Stem Cells* 2019; **11**: 831-858 [PMID: 31692971 DOI: 10.4252/wjsc.v11.i10.831]

67 **Solakoglu Ö**, Götz W, Kiessling MC, Alt C, Schmitz C, Alt EU. Improved guided bone regeneration by combined application of unmodified, fresh autologous adipose derived regenerative cells and plasma rich in growth factors: A first-in-human case report and literature review. *World J Stem Cells* 2019; **11**: 124-146 [PMID: 30842809 DOI: 10.4252/wjsc.v11.i2.124]

68 **Connor DE**, Paulus JA, Dabestani PJ, Thankam FK, Dilisio MF, Gross RM, Agrawal DK. Therapeutic potential of exosomes in rotator cuff tendon healing. *J Bone Miner Metab* 2019; **37**: 759-767 [PMID: 31154535 DOI: 10.1007/s00774-019-01013-z]

69 **Zhang M**, Liu H, Cui Q, Han P, Yang S, Shi M, Zhang T, Zhang Z, Li Z. Tendon stem cell-derived exosomes regulate inflammation and promote the high-quality healing of injured tendon. *Stem Cell Res Ther* 2020; **11**: 402 [PMID: 32943109 DOI: 10.1186/s13287-020-01918-x]

70 **Yu H**, Cheng J, Shi W, Ren B, Zhao F, Shi Y, Yang P, Duan X, Zhang J, Fu X, Hu X, Ao Y. Bone marrow mesenchymal stem cell-derived exosomes promote tendon regeneration by facilitating the proliferation and migration of endogenous tendon stem/progenitor cells. *Acta Biomater* 2020; **106**: 328-341 [PMID: 32027991 DOI: 10.1016/j.actbio.2020.01.051]

71 **Rhatomy S**, Prasetyo TE, Setyawan R, Soekarno NR, Romaniyanto F, Sedjati AP, Sumarwoto T, Utomo DN, Suroto H, Mahyudin F, Prakoeswa CRS. Prospect of stem cells conditioned medium (secretome) in ligament and tendon healing: A systematic review. *Stem Cells Transl Med* 2020; **9**: 895-902 [PMID: 32304180 DOI: 10.1002/sctm.19-0388]

72 **Hurd J**. Autologous adult adipose-derived regenerative cell injection into chronic partial-thickness rotator cuff tears. [accessed 2020 Dec 25]. In: ClinicalTrials.gov [Internet]. Identifier: NCT03752827. Available from: URL: https://www.clinicaltrials.gov/ct2/show/NCT03752827